

Correlation between the strength of low-temperature T-linear resistivity and T_c in overdoped electron-doped cuprate superconductors

Xingyu Ma^a, Minghuan Zeng^b, Huaiming Guo^c, and Shiping Feng^{a*}

^a*Department of Physics, Faculty of Arts and Sciences,
Beijing Normal University, Zhuhai 519087, China and*

School of Physics and Astronomy, Beijing Normal University, Beijing 100875, China

^b*College of Physics, Chongqing University, Chongqing 401331, China and*

^c*School of Physics, Beihang University, Beijing 100191, China*

The recently observed an intimate link between the nature of the strange metallic normal-state and superconductivity in the overdoped electron-doped cuprate superconductors is calling for an explanation. Here the intrinsic correlation between the strength of the low-temperature linear-in-temperature (T-linear) resistivity and superconducting transition temperature T_c in the overdoped electron-doped cuprate superconductors is studied within the framework of the kinetic-energy-driven superconductivity. On the one hand, the main ingredient is identified into a electron pairing mechanism involving *the spin excitation*, and then T_c has a dome-like shape doping dependence with the maximal T_c that occurs at around the optimal electron doping. On the other hand, in the normal-state above T_c , the low-temperature T-linear resistivity in the overdoped regime arises from the momentum relaxation due to the electron umklapp scattering mediated by *the same spin excitation*. This *same spin excitation* that governs both the electron umklapp scattering responsible for the low-temperature T-linear resistivity and electron pairing responsible for superconductivity naturally generates a correlation between the strength of the low-temperature T-linear resistivity and T_c in the overdoped regime.

PACS numbers: 74.25.Fy, 74.25.Nf, 74.20.Mn, 74.72.-h

Keywords: T-linear resistivity; Superconducting transition temperature; Electron umklapp scattering; Spin excitation; Electron-doped cuprate superconductors

I. INTRODUCTION

The undoped parent compounds of cuprate superconductors are antiferromagnetic (AF) Mott insulators¹, which result from the particularly strong electron correlation². However, the exceptionally strong superconductivity can be achieved when the AF long-range order (AFLRO) is destroyed by a small fraction of the electron or hole doping concentration^{3,4}. In particular, although both the electron doping and annealing process in a low-oxygen environment are required to induce superconductivity in the electron-doped cuprate superconductors⁵⁻⁷, the experimental observations demonstrate unambiguously that in a optimal annealing condition, the superconducting (SC) phase is extended over a wide electron doping range⁸⁻¹¹. In the recent measurements on the electron-doped cuprate superconductor $\text{Pr}_{1-x}\text{LaCe}_x\text{CuO}_{4-\delta}$ under the proper annealing condition⁹, it was observed experimentally that the SC transition temperature T_c reaches its maximum at around the optimal electron doping $\delta \sim 0.15$, while the disappearance of AFLRO at the doping is coincident with the onset of superconductivity, and hence the deduced AFLRO phase boundary does not extend into the SC dome. However, the very recent results^{10,11} observed experimentally the electron-doped cuprate superconductor $\text{Pr}_{1.3-x}\text{La}_{0.7}\text{Ce}_x\text{CuO}_{4-\delta}$ under the protect annealing condition indicated that the actual electron doping concentration estimated from the electron Fermi surface (EFS) area is significantly larger than the

Ce doping concentration x , and then the new electron-doping-based SC dome is more extended towards the overdoped side than the Ce-doping-based SC dome obtained for samples prepared in the proper annealing condition⁹. In particular, although the maximal T_c occurs at the optimally doped regime, this optimally doped regime spans a narrow doped range centered at around the doping $\delta \sim 0.15$ ¹⁰. Moreover, in the underdoped regime, T_c drops rapidly and vanishes at around the doping $\delta \sim 0.10$, while the AF correlation is found to coexist with superconductivity¹⁰. Since the dramatic suppression of the AFLRO has been observed in the underdoped regime of the electron-doped cuprate superconductors under the protect annealing condition⁸, one may anticipate a T_c recovery for $\delta \leq 0.10$ with further improved condition of the protect annealing¹⁰. These experimental results of the phase diagram for the electron-doped cuprate superconductors show that although some features in the underdoped regime observed in Ref.⁹ are significantly different from that in Ref.¹⁰, the doping range of these phase diagrams⁸⁻¹¹ bear a striking similarity to that of the corresponding phase diagram in the hole-doped counterparts^{12,13}, providing a clue for understanding the symmetry/asymmetry of the phase diagrams of the electron- and hole-doped cuprate superconductors. This similarity of the phase diagrams⁸⁻¹³ also suggests that the essential physics, including the SC mechanism and the nature of the normal-state in *the overdoped regime*, is most likely the same for both the electron- and hole-doped cuprate superconductors.

After intensive investigations over thirty years, a sub-

stantial amount of reliable and reproducible data for the electron-doped cuprate superconductors has been accumulated through systematic measurements using various techniques^{13–23}, which indicate that the normal-state property of these materials is a remarkable mystery and the most important unsolved problem in condensed matter physics. In particular, the normal-state property^{17–23} in the overdoped regime deviates from the conventional Fermi-liquid behavior^{24–26}. This has led to the normal-state in the overdoped regime being referred to as *the strange metallic normal-state*^{27–29}. One of the key manifestations of this deviation is the low-temperature linear-in-temperature (T-linear) resistivity, which persists down to millikelvin temperatures and extrapolates to zero resistivity at zero temperature^{17–23}. Recently, this low-temperature T-linear resistivity in the overdoped electron-doped cuprate superconductors has been confirmed experimentally all the way up to the edge of the SC dome²³. More importantly, these experimental observations also establish definitively that in the overdoped regime, the low-temperature T-linear resistivity is tied to T_c , where the strength of the low-temperature T-linear resistivity (then the T-linear resistivity coefficient) follows a scaling relation with the corresponding magnitude of T_c , and then the strength of the low-temperature T-linear resistivity decreases as T_c decreases. This surprising correlation between the strength of the low-temperature T-linear resistivity and the corresponding magnitude of T_c in the overdoped electron-doped cuprate superconductors^{17–23} therefore strongly suggests an intimate link between the nature of the strange metallic normal-state and superconductivity. In other words, the origin of the strange metallic normal-state is intertwined with the origin of superconductivity. In this case, the strange metallic normal-state of the overdoped electron-doped cuprate superconductors potentially serves as a starting point for a deep understanding of the SC mechanism of cuprate superconductivity.

Although the intrinsic correlation between the strength of the low-temperature T-linear resistivity and the corresponding magnitude of T_c in the overdoped electron-doped cuprate superconductors has been established experimentally^{19–23}, a complete understanding of this correlation is still unclear. In particular, a key question is whether a common bosonic excitation, which dominates both the electron scattering responsible for the low-temperature T-linear resistivity and the electron pairing responsible for superconductivity, makes a correlation between the strength of the low-temperature T-linear resistivity and the corresponding magnitude of T_c . In the recent work³⁰, the doping-temperature phase diagram in the electron-doped cuprate superconductors was discussed based on the kinetic-energy-driven SC mechanism, where the main ingredient is identified into the constrained electron pairing mechanism involving *the spin excitation, the collective mode from the internal spin degree of freedom of the constrained electron itself*. In this

case, the obtained T_c increases with the increase of electron doping in the underdoped regime, and reaches its maximum in the optimal electron doping, then decreases in the overdoped regime³⁰. On the other hand, the nature of the low-temperature T-linear resistivity in the overdoped hole-doped cuprate superconductors was investigated very recently³¹, where the electron umklapp scattering from the spin excitation can give a consistent description of the low-temperature T-linear resistivity. In particular, a very low temperature T_{scale} scales with Δ_p^2 , where Δ_p is the minimal umklapp vector at the antinode, and then above T_{scale} , the resistivity is T-linear with the strength that decreases with the increase of hole doping. In this paper, we study the remarkable correlation between the strength of the low-temperature T-linear resistivity and the corresponding magnitude of T_c in the overdoped electron-doped cuprate superconductors along with these lines. We identify explicitly that the momentum relaxation due to the electron umklapp scattering mediated by the spin excitation reveals itself in the nature of the low-temperature T-linear resistivity in the overdoped electron-doped cuprate superconductors as it works in the overdoped hole-doped counterparts³¹. Our results in this paper together with the previous work for superconductivity³⁰ therefore indicate a fact: the *spin excitation* that mediates the attractive interaction between the electrons responsible for superconductivity also mediates the electron umklapp scattering responsible for the low-temperature T-linear resistivity in the overdoped regime. This *same spin excitation* then generates naturally a striking correlation between the strength of the low-temperature T-linear resistivity and the corresponding magnitude of T_c in the overdoped electron-doped cuprate superconductors.

This paper is organized as follows. The theoretical framework is presented in Sec. II, where a brief review of the doping-temperature phase diagram of the electron-doped cuprate superconductors is given for the convenience in the discussions of the correlation between the strength of the low-temperature T-linear resistivity and the corresponding magnitude of T_c in the overdoped electron-doped cuprate superconductors. The transport scattering rate, however, is obtained in terms of the spin-excitation-mediated electron umklapp scattering, and is used to derive the resistivity within the framework of the Boltzmann transport theory. The quantitative characteristics of the correlation between the strength of the low-temperature T-linear resistivity and the corresponding magnitude of T_c in the overdoped regime are presented in Section III, where it is shown that as in the hole-doped case³¹, the resistivity in the overdoped electron-doped cuprate superconductors also exhibits a crossover from the T-linear behaviour in the low-temperature region into the quadratic in temperature (T-quadratic) behaviour in the far lower temperature region. Finally, we give a summary in Sec. IV. In the Appendix A, we present the generalization of the main formalisms of the kinetic-energy-driven superconductivity from the hole-doped case to the

present electron-doped case, where the detail of the calculation of the doping dependence of T_c is given.

II. THEORETICAL FORMALISM

A. Model and electron local constraint

The basic element of the crystal structure of both the electron- and hole-doped cuprate superconductors is the square-lattice copper-oxide plane in which superconductivity occurs upon either electron or hole doping^{3,4}. As in the hole-doped case², the various signature features of the electron-doped cuprate superconductors can be also properly captured by the t - J model on a square lattice,

$$H = -t \sum_{\langle ll' \rangle \sigma} C_{l\sigma}^\dagger C_{l'\sigma} + t' \sum_{\langle\langle ll' \rangle\rangle \sigma} C_{l\sigma}^\dagger C_{l'\sigma} + \mu \sum_{l\sigma} C_{l\sigma}^\dagger C_{l\sigma} + J \sum_{\langle ll' \rangle} \mathbf{S}_l \cdot \mathbf{S}_{l'}, \quad (1)$$

where $C_{l\sigma}^\dagger$ ($C_{l\sigma}$) creates (annihilates) an electron with spin σ (either \uparrow or \downarrow) on site l , \mathbf{S}_l is a localized spin operator with its components S_l^x , S_l^y , and S_l^z , while the chemical potential μ fixes the total number of electrons. The angle brackets $\langle ll' \rangle$ and $\langle\langle ll' \rangle\rangle$ indicate the summations over the nearest-neighbor (NN) and next NN pairs, respectively. The t - J model with the NN hopping t has a particle-hole symmetry since the sign of t can be absorbed by the change of the sign of the orbital on one sublattice³²⁻³⁴. However, the particle-hole asymmetry can be properly described by the next NN hopping t' , which has been tested extensively³²⁻³⁴. In particular, it has been shown clearly that the asymmetry seen by the angle-resolved photoemission spectroscopy (ARPES) observation on the hole-doped and electron-doped cuprate superconductors is actually consistent with calculations³⁴ performed within the t - J model (1), where all of the hopping terms have opposite signs for the electron and hole doping, while the sign of t' is of crucial importance for the coupling of the charge motion to the spin background³²⁻³⁴. Throughout this paper, the NN magnetic exchange coupling J is set as the energy unit, and t and t' are set to $t/J = -2.5$ and $t'/t = 0.3$, respectively, as in the previous discussions of the low-energy electronic structure of the electron-doped cuprate superconductors³⁰. However, to compare with the experimental energy scales, we set $J = 1000\text{K}$.

This t - J model (1) is the strong coupling limit of the Hubbard model, and then the crucial difficulty of its solution lies in enforcing the electron on-site local constraint³⁵⁻³⁸, i.e., this t - J model (1) is subject to a on-site local constraint of no double electron occupancy in the hole-doped case: $\sum_{\sigma} C_{l\sigma}^\dagger C_{l\sigma} \leq 1$, while it is subject a on-site local constraint of no zero electron occupancy in the electron-doped side: $\sum_{\sigma} C_{l\sigma}^\dagger C_{l\sigma} \geq 1$. In the hole-doped case, the fermion-spin transformation^{39,40} has been developed, where the on-site local constraint

of no double electron occupancy can be treated properly in the actual analyses. To apply this fermion-spin transformation^{39,40} to the electron-doped case, the t - J model (1) in the electron representation can be converted into the t - J model in the hole representation by virtue of a particle-hole transformation $C_{l\sigma} \rightarrow f_{l-\sigma}^\dagger$ as³⁰,

$$H = t \sum_{\langle ll' \rangle \sigma} f_{l\sigma}^\dagger f_{l'\sigma} - t' \sum_{\langle\langle ll' \rangle\rangle \sigma} f_{l\sigma}^\dagger f_{l'\sigma} - \mu_f \sum_{l\sigma} f_{l\sigma}^\dagger f_{l\sigma} + J \sum_{\langle ll' \rangle} \mathbf{S}_l \cdot \mathbf{S}_{l'}, \quad (2)$$

where $f_{l\sigma}^\dagger$ ($f_{l\sigma}$) is the creation (annihilation) operator for a hole on site l with spin σ . Concomitantly, the on-site local constraint of no zero electron occupancy in the electron representation $\sum_{\sigma} C_{l\sigma}^\dagger C_{l\sigma} \geq 1$ is transformed into the on-site local constraint of no double hole occupancy in the hole representation $\sum_{\sigma} f_{l\sigma}^\dagger f_{l\sigma} \leq 1$. In this case, the t - J model (1) in both the electron- and hole-doped cases is always subject to a on-site local constraint that double occupancy of a site by two fermions of opposite spins is not allowed, while the difference between the electron doping and hole doping is reflected in the sign difference of the hopping integrals as we have mentioned above. The physics of the no double occupancy in the fermion-spin transformation^{39,40} is taken into account by representing the fermion operator $f_{l\sigma}$ as a composite object created by,

$$f_{l\uparrow} = a_{l\uparrow}^\dagger S_l^-, \quad f_{l\downarrow} = a_{l\downarrow}^\dagger S_l^+, \quad (3)$$

and then the on-site local constraint of no double occupancy is satisfied in actual analyses. The $U(1)$ gauge invariant spinful fermion operator $a_{l\sigma}^\dagger = e^{i\Phi_{l\sigma}} a_l^\dagger$ ($a_{l\sigma} = e^{-i\Phi_{l\sigma}} a_l$) creates (annihilates) a charge carrier on site l , and therefore keeps track of the charge degree of freedom of the constrained electron together with some effects of spin configuration rearrangements due to the presence of the doped electron itself. However, the $U(1)$ gauge invariant spin operator S_l^+ (S_l^-) keeps track of the spin degree of freedom of the constrained electron, and therefore the collective mode from this spin degree of freedom of the constrained electron can be interpreted as the spin excitation responsible for the dynamical spin response of the system. In this fermion-spin representation (3), the t - J model (2) can be expressed as,

$$H = -t \sum_{\langle ll' \rangle} (a_{l\uparrow}^\dagger a_{l'\uparrow} S_{l'}^+ S_l^- + a_{l\downarrow}^\dagger a_{l'\downarrow} S_{l'}^- S_l^+) + t' \sum_{\langle\langle ll' \rangle\rangle} (a_{l\uparrow}^\dagger a_{l'\uparrow} S_{l'}^+ S_l^- + a_{l\downarrow}^\dagger a_{l'\downarrow} S_{l'}^- S_l^+) + \mu_a \sum_{l\sigma} a_{l\sigma}^\dagger a_{l\sigma} + J_{\text{eff}} \sum_{\langle ll' \rangle} \mathbf{S}_l \cdot \mathbf{S}_{l'}, \quad (4)$$

with $J_{\text{eff}} = (1 - \delta)^2 J$, and the doping concentration $\delta = \langle a_{l\sigma}^\dagger a_{l\sigma} \rangle = \langle a_l^\dagger a_l \rangle$. As in the hole-doped case³¹, the kinetic-energy term in the t - J model (4) in the fermion-spin representation has been transformed into the strong

coupling between charge and spin degrees of freedom of the constrained electron, and thus governs the essential physics in the electron-doped cuprate superconductors.

B. Kinetic-energy-driven superconductivity

In the early days of superconductivity research, the kinetic-energy-driven SC mechanism for the hole-doped cuprate superconductors^{40–43} was established based on the t - J model in the fermion-spin representation. In this kinetic-energy-driven superconductivity, the spin-excitation-mediated attractive interaction, which pairs the charge carriers together to form the d-wave charge-carrier pairing state, arises directly from the coupling of the charge and spin degrees of freedom of the constrained electron in the kinetic energy of the t - J model. However, the electron pairs with the d-wave symmetry are generated from this d-wave charge-carrier pairing state in terms of the charge-spin recombination⁴³, and then the condensation of these electron pairs reveals the d-wave SC ground-state. This kinetic-energy-driven SC mechanism reveals that (i) the constrained electron has dual roles, since the glue to hold the constrained electron pairs together is *the spin excitation, the collective mode from the spin degree of freedom of the constrained electron itself*. In other words, the constrained electrons simultaneously act to glue and to be glued^{44,45}; (ii) the spin-excitation-mediated electron pairing state in a way is in turn strongly influenced by the single-particle coherence, leading to a dome-like shape doping dependence of T_c . Starting from the t - J model (4) in the fermion-spin representation, the formalism of the kinetic-energy-driven superconductivity developed for the hole-doped case has been generalized to the electron-doped side^{30,46}, where the complicated line-shape in the energy distribution curve, the kink in the electron dispersion, and the autocorrelation of the angle-resolved photoemission spectroscopy have been discussed, and the obtained results are well consistent with the corresponding experimental results^{8–11}. Our following discussions of the correlation between the strength of the low-temperature T-linear resistivity and the corresponding magnitude of T_c in the overdoped electron-doped cuprate superconductors builds on the kinetic-energy-driven SC mechanism. For the following discussions of the main physics in the core, the details of the derivation of the main formalisms of the kinetic-energy-driven superconductivity in the electron-doped case are presented in Appendix A. In the previous discussions^{30,46}, the full hole diagonal and off-diagonal propagators $G_f(\mathbf{k}, \omega)$ and $\mathfrak{S}_f^\dagger(\mathbf{k}, \omega)$ of the t - J model (4) in the fermion-spin representation that satisfy the self-consistent Dyson's equations have been obtained in terms of the Eliashberg's approach⁴⁷ as [see Appendix A],

$$G_f(\mathbf{k}, \omega) = \frac{1}{\omega - \varepsilon_{\mathbf{k}}^{(f)} - \Sigma_{\text{tot}}^{(f)}(\mathbf{k}, \omega)}, \quad (5a)$$

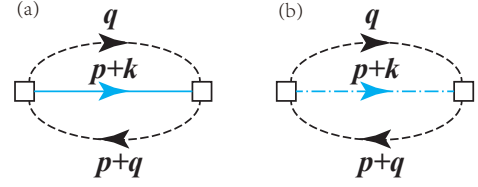


FIG. 1. The skeletal diagrams for the hole (a) normal and (b) anomalous self-energies for scattering holes from the spin excitation. The blue-solid-line and blue-dash-dot-line represent the hole diagonal and off-diagonal propagators G_f and \mathfrak{S}_f^\dagger , respectively, and the black-dash-line depicts the spin propagator $D^{(0)}$, while \square describes the vertex function Λ .

$$\mathfrak{S}_f^\dagger(\mathbf{k}, \omega) = \frac{L^{(f)}(\mathbf{k}, \omega)}{\omega - \varepsilon_{\mathbf{k}}^{(f)} - \Sigma_{\text{tot}}^{(f)}(\mathbf{k}, \omega)}, \quad (5b)$$

where the non-interaction band energy $\varepsilon_{\mathbf{k}}^{(f)} = 4t\gamma_{\mathbf{k}} - 4t'\gamma'_{\mathbf{k}} - \mu$, with $\gamma_{\mathbf{k}} = (\cos k_x + \cos k_y)/2$ and $\gamma'_{\mathbf{k}} = \cos k_x \cos k_y$, while the total hole self-energy $\Sigma_{\text{tot}}^{(f)}(\mathbf{k}, \omega)$ and the function $L^{(f)}(\mathbf{k}, \omega)$ are respectively given by,

$$\Sigma_{\text{tot}}^{(f)}(\mathbf{k}, \omega) = \Sigma_{\text{ph}}^{(f)}(\mathbf{k}, \omega) + \frac{|\Sigma_{\text{pp}}^{(f)}(\mathbf{k}, \omega)|^2}{\omega + \varepsilon_{\mathbf{k}}^{(f)} + \Sigma_{\text{ph}}^{(f)}(\mathbf{k}, -\omega)}, \quad (6a)$$

$$L^{(f)}(\mathbf{k}, \omega) = -\frac{\Sigma_{\text{pp}}^{(f)}(\mathbf{k}, \omega)}{\omega + \varepsilon_{\mathbf{k}}^{(f)} + \Sigma_{\text{ph}}^{(f)}(\mathbf{k}, -\omega)}. \quad (6b)$$

The hole normal self-energy $\Sigma_{\text{ph}}^{(f)}(\mathbf{k}, \omega)$ in the particle-hole channel sketched in Fig. 1a and the hole anomalous self-energy $\Sigma_{\text{pp}}^{(f)}(\mathbf{k}, \omega)$ in the particle-particle channel sketched in Fig. 1b have been derived in terms of the full hole diagonal and off-diagonal propagators as [see Appendix A],

$$\Sigma_{\text{ph}}^{(f)}(\mathbf{k}, i\omega_n) = \frac{1}{N} \sum_{\mathbf{p}} \frac{1}{\beta} \sum_{ip_m} G_f(\mathbf{p} + \mathbf{k}, ip_m + i\omega_n) \times P^{(0)}(\mathbf{k}, \mathbf{p}, ip_m), \quad (7a)$$

$$\Sigma_{\text{pp}}^{(f)}(\mathbf{k}, i\omega_n) = \frac{1}{N} \sum_{\mathbf{p}} \frac{1}{\beta} \sum_{ip_m} \mathfrak{S}_f^\dagger(\mathbf{p} + \mathbf{k}, ip_m + i\omega_n) \times P^{(0)}(\mathbf{k}, \mathbf{p}, ip_m), \quad (7b)$$

respectively, with the number of lattice sites N , the fermionic and bosonic Matsubara frequencies ω_n and p_m , respectively, and the effective spin propagator,

$$P^{(0)}(\mathbf{k}, \mathbf{p}, \omega) = \frac{1}{N} \sum_{\mathbf{q}} \Lambda_{\mathbf{p}+\mathbf{q}+\mathbf{k}}^2 \Pi(\mathbf{p}, \mathbf{q}, \omega), \quad (8)$$

where $\Lambda_{\mathbf{k}} = 4t\gamma_{\mathbf{k}} - 4t'\gamma'_{\mathbf{k}}$ is the vertex function. This effective spin propagator $P^{(0)}(\mathbf{k}, \mathbf{p}, \omega)$ depict the nature of the spin excitation, and is directly associated with the spin bubble $\Pi(\mathbf{p}, \mathbf{q}, \omega)$, while this spin bubble $\Pi(\mathbf{p}, \mathbf{q}, \omega)$

is a convolution of two spin propagators, and can be expressed as,

$$\Pi(\mathbf{p}, \mathbf{q}, ip_m) = \frac{1}{\beta} \sum_{iq_m} D^{(0)}(\mathbf{q}, iq_m) D^{(0)}(\mathbf{q}+\mathbf{p}, iq_m+ip_m), \quad (9)$$

with the bosonic Matsubara frequency q_m , and the spin propagator⁴⁸,

$$D^{(0)}(\mathbf{k}, \omega) = \frac{B_{\mathbf{k}}}{\omega^2 - \omega_{\mathbf{k}}^2} = \frac{B_{\mathbf{k}}}{2\omega_{\mathbf{k}}} \left(\frac{1}{\omega - \omega_{\mathbf{k}}} - \frac{1}{\omega + \omega_{\mathbf{k}}} \right), \quad (10)$$

where the weight function of the spin excitation spectrum $B_{\mathbf{k}}$ and the spin excitation energy dispersion $\omega_{\mathbf{k}}$ have been given explicitly in Appendix A.

With the help of the above spin propagator in Eq. (10), the spin bubble $\Pi(\mathbf{p}, \mathbf{q}, \omega)$ in Eq. (9) can be evaluated as,

$$\Pi(\mathbf{p}, \mathbf{q}, ip_m) = -\frac{\bar{W}_{\mathbf{p}\mathbf{q}}^{(1)}}{(ip_m)^2 - [\omega_{\mathbf{p}\mathbf{q}}^{(1)}]^2} + \frac{\bar{W}_{\mathbf{p}\mathbf{q}}^{(2)}}{(ip_m)^2 - [\omega_{\mathbf{p}\mathbf{q}}^{(2)}]^2}, \quad (11)$$

with $\omega_{\mathbf{p}\mathbf{q}}^{(1)} = \omega_{\mathbf{q}+\mathbf{p}} + \omega_{\mathbf{q}}$, $\omega_{\mathbf{p}\mathbf{q}}^{(2)} = \omega_{\mathbf{q}+\mathbf{p}} - \omega_{\mathbf{q}}$, and the functions,

$$\bar{W}_{\mathbf{p}\mathbf{q}}^{(1)} = \frac{B_{\mathbf{q}}B_{\mathbf{q}+\mathbf{p}}}{2\omega_{\mathbf{q}}\omega_{\mathbf{q}+\mathbf{p}}} \omega_{\mathbf{p}\mathbf{q}}^{(1)} [n_B(\omega_{\mathbf{q}+\mathbf{p}}) + n_B(\omega_{\mathbf{q}}) + 1], \quad (12a)$$

$$\bar{W}_{\mathbf{p}\mathbf{q}}^{(2)} = \frac{B_{\mathbf{q}}B_{\mathbf{q}+\mathbf{p}}}{2\omega_{\mathbf{q}}\omega_{\mathbf{q}+\mathbf{p}}} \omega_{\mathbf{p}\mathbf{q}}^{(2)} [n_B(\omega_{\mathbf{q}+\mathbf{p}}) - n_B(\omega_{\mathbf{q}})], \quad (12b)$$

where $n_B(\omega)$ is the boson distribution function, and then the effective spin propagator $P^{(0)}(\mathbf{k}, \mathbf{p}, \omega)$ in Eq. (8) is obtained directly from the above spin bubble in Eq. (11). Substituting the effective spin propagator in Eq. (8) into Eq. (7), the hole normal and anomalous self-energies $\Sigma_{\text{ph}}^{(f)}(\mathbf{k}, \omega)$ and $\Sigma_{\text{pp}}^{(f)}(\mathbf{k}, \omega)$ can be derived straightforwardly, and have been given explicitly in Appendix A.

However, for the discussions of a link between the nature of the strange metallic normal-state and superconductivity in the overdoped electron-doped cuprate superconductors, we need to derive the full electron diagonal and off-diagonal propagators $G(\mathbf{k}, \omega)$ and $\mathfrak{S}^\dagger(\mathbf{k}, \omega)$. These full electron diagonal and off-diagonal propagators $G(\mathbf{k}, \omega)$ and $\mathfrak{S}^\dagger(\mathbf{k}, \omega)$ are respectively associated with the hole diagonal and off-diagonal propagators $G_f(\mathbf{k}, \omega)$ and $\mathfrak{S}_f^\dagger(\mathbf{k}, \omega)$ in Eq. (5) via the particle-hole transformation $C_{l\sigma} \rightarrow f_{l-\sigma}^\dagger$ as $G(l-l', t-t') = \langle\langle C_{l\sigma}(t); C_{l'\sigma}^\dagger(t') \rangle\rangle = \langle\langle f_{l\sigma}^\dagger(t); f_{l'\sigma}(t') \rangle\rangle = -G_f(l-l', t-t')$ and $\mathfrak{S}(l-l', t-t') = \langle\langle C_{l\downarrow}(t); C_{l'\uparrow}(t') \rangle\rangle = \langle\langle f_{l\uparrow}^\dagger(t); f_{l'\downarrow}^\dagger(t') \rangle\rangle = \mathfrak{S}_f^\dagger(l-l', t-t')$, and have been obtained explicitly as^{30,46},

$$G(\mathbf{k}, \omega) = \frac{1}{\omega - \varepsilon_{\mathbf{k}} - \Sigma_{\text{tot}}(\mathbf{k}, \omega)}, \quad (13a)$$

$$\mathfrak{S}^\dagger(\mathbf{k}, \omega) = \frac{L(\mathbf{k}, \omega)}{\omega - \varepsilon_{\mathbf{k}} - \Sigma_{\text{tot}}(\mathbf{k}, \omega)}, \quad (13b)$$

where the electron non-interaction band energy $\varepsilon_{\mathbf{k}} = -\varepsilon_{\mathbf{k}}^{(f)} = -4t\gamma_{\mathbf{k}} + 4t'\gamma'_{\mathbf{k}} + \mu$, while the electron total self-

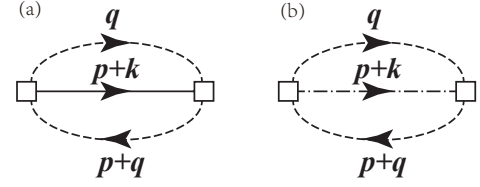


FIG. 2. The skeletal diagrams for the electron (a) normal and (b) anomalous self-energies for scattering electrons from the spin excitation. The black-solid-line and black-dash-dot-line represent the electron diagonal and off-diagonal propagators G and \mathfrak{S}^\dagger , respectively, and the black-dash-line depicts the spin propagator $D^{(0)}$, while \square describes the vertex function Λ .

energy $\Sigma_{\text{tot}}(\mathbf{k}, \omega)$ and the function $L(\mathbf{k}, \omega)$ can be expressed explicitly as,

$$\Sigma_{\text{tot}}(\mathbf{k}, \omega) = \Sigma_{\text{ph}}(\mathbf{k}, \omega) + \frac{|\Sigma_{\text{pp}}(\mathbf{k}, \omega)|^2}{\omega + \varepsilon_{\mathbf{k}} + \Sigma_{\text{ph}}(\mathbf{k}, -\omega)}, \quad (14a)$$

$$L(\mathbf{k}, \omega) = -\frac{\Sigma_{\text{pp}}(\mathbf{k}, \omega)}{\omega + \varepsilon_{\mathbf{k}} + \Sigma_{\text{ph}}(\mathbf{k}, -\omega)}, \quad (14b)$$

respectively, with the electron normal self-energy $\Sigma_{\text{ph}}(\mathbf{k}, \omega)$ sketched in Fig. 2a and electron anomalous self-energy $\Sigma_{\text{pp}}(\mathbf{k}, \omega)$ sketched in Fig. 2b that have been obtained straightforwardly as^{30,46},

$$\Sigma_{\text{ph}}(\mathbf{k}, \omega) = -\Sigma_{\text{ph}}^{(f)}(\mathbf{k}, -\omega), \quad (15a)$$

$$\Sigma_{\text{pp}}(\mathbf{k}, \omega) = \Sigma_{\text{pp}}^{(f)}(\mathbf{k}, \omega), \quad (15b)$$

respectively. Moreover, the sharp peaks appear at low-temperature in $\Sigma_{\text{ph}}(\mathbf{k}, \omega)$, $\Sigma_{\text{pp}}(\mathbf{k}, \omega)$, and $P^{(0)}(\mathbf{k}, \mathbf{p}, \omega)$ are actually a δ -function that are broadened by a small damping employed in the numerical calculation for a finite lattice^{49,50}. As the approach described in Ref.³⁰, the calculation in this paper for $\Sigma_{\text{ph}}(\mathbf{k}, \omega)$, $\Sigma_{\text{pp}}(\mathbf{k}, \omega)$, and $P^{(0)}(\mathbf{k}, \mathbf{p}, \omega)$ is performed numerically on a 160×160 lattice in momentum space, where the infinitesimal $i0_+ \rightarrow i\Gamma$ is replaced by a small damping $\Gamma = 0.1J$.

C. Doping dependence of T_c

Based on the kinetic-energy-driven SC mechanism discussed in the above subsection II B, the evolution of T_c with the electron doping in the electron-doped cuprate superconductors³⁰ has been investigated recently by making use of the self-consistent calculation in the condition of the SC gap $\bar{\Delta}(\mathbf{k}) = \Sigma_{\text{pp}}(\mathbf{k}, 0) = 0$ [see Appendix A]. For the convenience in the discussions of the correlation between the strength of the low-temperature T-linear resistivity and the corresponding magnitude of T_c in the overdoped electron-doped cuprate superconductors, the result of T_c as a function of the electron doping is

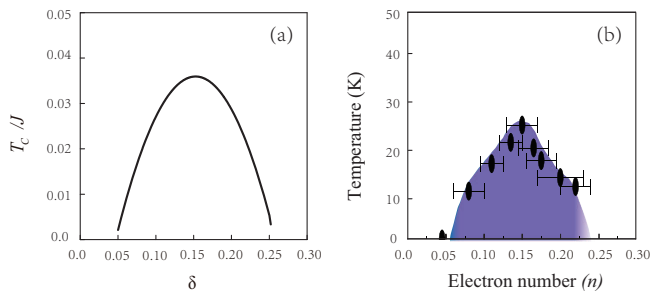


FIG. 3. (Color online) (a) Doping dependence of T_c . (b) The corresponding experimental result observed on $\text{Pr}_{1-x}\text{LaCe}_x\text{CuO}_{4-\delta}$ under the proper annealing condition taken from Ref. 9.

replotted in Fig. 3a. For a better comparison, the corresponding experimental result⁹ observed on the electron-doped cuprate superconductor $\text{Pr}_{1-x}\text{LaCe}_x\text{CuO}_{4-\delta}$ under the proper annealing condition is also shown in Fig. 3b. Apparently, the experimental result⁹ of the doping dependent T_c in $\text{Pr}_{1-x}\text{LaCe}_x\text{CuO}_{4-\delta}$ under the proper annealing condition is qualitatively reproduced, where the gradual increase in T_c with the increase of the electron doping occurs in the underdoped regime, and T_c reaches its maximum at around the optimal electron doping $\delta \sim 0.15$, subsequently, T_c decreases monotonically with the increase of the electron doping in the overdoped regime. In comparison with the corresponding result for the hole-doped case^{12,13,43}, it thus shows that although the magnitude of the optimized T_c in the electron-doped side is much lower than that in the hole-doped case, the doping range of the SC dome in the electron-doped side is in a striking analogy with that in the hole-doped case^{12,13,43}, and in this sense, the absence of the disparity between the phase diagrams of the electron- and hole-doped cuprate superconductors⁸⁻¹³ is therefore confirmed.

D. Electron Fermi surface

The transition from the SC-state to the normal-state manifest in the anomalous self-energy (then the full electron off-diagonal propagator) becomes zero above T_c , and then the full electron propagator in Eq. (13) in the SC-state is reduced in the normal-state as,

$$G(\mathbf{k}, \omega) = \frac{1}{\omega - \varepsilon_{\mathbf{k}} - \Sigma_{\text{ph}}(\mathbf{k}, \omega)}, \quad (16)$$

while the electron spectrum function $A(\mathbf{k}, \omega) = -\text{Im}G(\mathbf{k}, \omega)/\pi$ is obtained directly as,

$$A(\mathbf{k}, \omega) = -\frac{1}{\pi} \frac{\text{Im}\Sigma_{\text{ph}}(\mathbf{k}, \omega)}{[\omega - \varepsilon_{\mathbf{k}} - \text{Re}\Sigma_{\text{ph}}(\mathbf{k}, \omega)]^2 + [\text{Im}\Sigma_{\text{ph}}(\mathbf{k}, \omega)]^2}, \quad (17)$$

where $\text{Re}\Sigma_{\text{ph}}(\mathbf{k}, \omega)$ and $\text{Im}\Sigma_{\text{ph}}(\mathbf{k}, \omega)$ are the real and imaginary parts of the electron normal self-energy

$\Sigma_{\text{ph}}(\mathbf{k}, \omega)$, respectively.

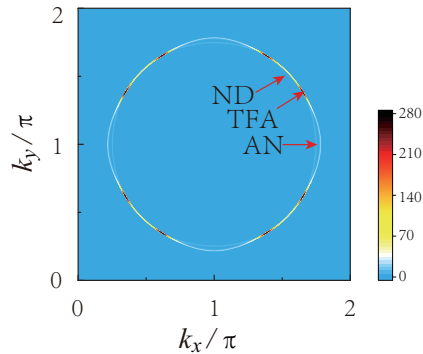


FIG. 4. (Color online) The map of the electron Fermi surface at $\delta = 0.19$ with $T = 0.002J$, where the Brillouin zone center has been shifted by $[\pi, \pi]$, and AN, TFA, and ND denote the antinode, tip of the Fermi arc, and node, respectively.

The electron Fermi surface (EFS) separates the occupied and unoccupied states, and therefore the geometrical structure of EFS is closely linked with the low-energy electronic structure^{5,51-53} as well as the electrical transport⁵⁴⁻⁵⁶. In the recent work⁵⁷, the geometrical structure of EFS in the electron-doped cuprate superconductors has been studied, where the underlying EFS is obtained via the map of the electron spectral function (17) at zero energy $\omega = 0$, i.e., the closed EFS contour is determined by the poles of the full electron propagator (16) at zero energy: $\varepsilon_{\mathbf{k}} + \text{Re}\Sigma_{\text{ph}}(\mathbf{k}, 0) = \bar{\varepsilon}_{\mathbf{k}} = 0$, with the renormalized electron energy dispersion $\bar{\varepsilon}_{\mathbf{k}} = Z_F \varepsilon_{\mathbf{k}}$ and the single-particle coherent weight $Z_F^{-1} = 1 - \text{Re}\Sigma_{\text{pho}}(\mathbf{k}, 0) |_{\mathbf{k}=[\pi, 0]}$, while $\Sigma_{\text{pho}}(\mathbf{k}, \omega)$ that is the antisymmetric part of the electron normal self-energy $\Sigma_{\text{ph}}(\mathbf{k}, \omega)$. However, the strong redistribution of the spectral weight at the closed EFS contour is dominated by the imaginary part of the electron normal self-energy $\text{Im}\Sigma_{\text{ph}}(\mathbf{k}, \omega)$ [then the single-particle scattering rate $\Gamma_{\mathbf{k}}(\omega) = |\text{Im}\Sigma_{\text{ph}}(\mathbf{k}, \omega)|$]. To see this point more clearly, we plot the EFS map at the electron doping $\delta = 0.19$ with temperature $T = 0.002J$ in Fig. 4, where the Brillouin zone (BZ) center has been shifted by $[\pi, \pi]$, and AN, TFA, and ND indicate the antinode, tip of the Fermi arc, and node, respectively. Our result in Fig. 4 therefore shows that EFS has been separated into three typical regions due to the strong redistribution of the spectral weight⁵⁷: (i) the antinodal region, where the spectral weight is reduced strongly, leading to EFS at around the antinodal region to become invisible; (ii) the nodal region, where the spectral weight is reduced moderately, leading to EFS to be clearly visible as the reminiscence of the EFS contour in the case of the absence of the electron interaction to form the Fermi arcs; (iii) the region at around the tips of the Fermi arcs, where the spectral weight exhibits the largest value. This EFS reconstruction is also qualitatively consistent with the recent experimental observations on the electron-doped cuprate superconductors⁸⁻¹¹, where upon the optimal an-

nealing, the weight of the ARPES spectrum around the antinodal region is reduced, and then EFS is truncated to form the Fermi arcs located around the nodal region.

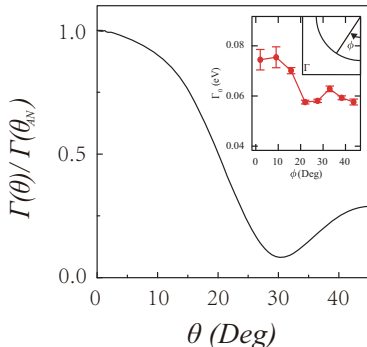


FIG. 5. The single-particle scattering rate $\Gamma(\theta)/\Gamma(\theta_{\text{AN}})$ as a function of Fermi angle θ at $\delta = 0.19$ with $T = 0.002J$ for $\omega = 0$, where $\Gamma(\theta_{\text{AN}})$ is the single-particle scattering rate at the antinode. Inset: the corresponding experimental result of the overdoped $\text{Pr}_{1.3-x}\text{La}_{0.7}\text{Ce}_x\text{CuO}_4$ taken from Ref. 8.

In the previous studies⁵⁷, it has been shown that the spectral redistribution to form the Fermi arcs is directly associated with the angular dependence of the single-particle scattering rate $\Gamma(\theta)$, where $\Gamma(\theta) = \Gamma_{\mathbf{k}_F(\theta)}(0) = |\text{Im}\Sigma_{\text{ph}}(\mathbf{k}_F(\theta), 0)|$ with the Fermi angle θ . To see this $\Gamma(\theta)$ in momentum space more clearly, we plot the $\Gamma(\theta)/\Gamma(\theta_{\text{AN}})$ along EFS from the antinode to the node at $\delta = 0.19$ with $T = 0.002J$ in Fig. 5, where $\Gamma(\theta_{\text{AN}})$ is the single-particle scattering rate at the antinode. For comparison, the corresponding experimental result of the single-particle scattering rate along EFS observed from the overdoped electron-doped cuprate superconductor⁸ $\text{Pr}_{1.3-x}\text{La}_{0.7}\text{Ce}_x\text{CuO}_4$ is also presented in Fig. 5 (inset). It thus shows that the actual minimum of $\Gamma(\theta)$ does not site at the node, but appears at around the tip of the Fermi arc. On the other hand, the magnitude of $\Gamma(\theta)$ still exhibits the largest value at the antinode, and then it decreases when the momentum moves away from the antinode. Moreover, the magnitude of $\Gamma(\theta)$ at the antinode is much larger than that at the node. This special angular dependence of $\Gamma(\theta)$ therefore generates a spectral redistribution to form the Fermi arcs with the largest value of the spectral weight located at around the tips of the Fermi arcs.

E. Momentum relaxation in the normal-state

We now turn to discuss the normal-state electrical transport in the overdoped electron-doped cuprate superconductors. As in the hole-doped case⁵¹⁻⁵³, the conventional quasiparticle picture breaks down in the normal-state of the overdoped electron-doped cuprate superconductors⁵. In this case, two different methods have been employed to investigate the electrical transport in the case of the lack of the well-defined quasi-

particle. The first one is the memory-matrix transport approach⁵⁸⁻⁶³, which has a distinct advantage of not relying on the existence of the well-defined quasiparticle. In particular, the electrical transports in the strange-metal phases of different strongly correlated systems have been investigated based on the memory-matrix transport approach⁵⁸⁻⁶³, and the obtained results are consistent with the corresponding experimental data. The another method employed is the Boltzmann transport theory^{25,26}, where it is crucial to assume either the validity of the conventional quasiparticle picture or the treatment of the electron interaction mediated by different bosonic modes within the Eliashberg approach^{64,65}. This follows a basic fact that (i) in the early pioneering work⁶⁴, Prange and Kadanoff have shown that in an electron-phonon system, a set of transport equations can be derived in the Migdal's approximation. In particular, this coupled set of transport equations for the electron and phonon distribution functions is correct even in the case in which the electron excitation spectrum has considerable width and structure so that one might not expect a priori that there would be the well-defined quasiparticle⁶⁴. Nevertheless, one of the forms of the electrical transport equation,

$$e\mathbf{E} \cdot \nabla_{\mathbf{k}} f(\mathbf{k}) = I_{e-e}, \quad (18)$$

is identical to the electrical transport equation proposed by Landau for the case of the existence of the well-defined quasiparticle^{25,26}, where e is the charge of an electron, and $f(\mathbf{k}, t)$ is the distribution function in a homogeneous system. For the convenience in the following discussions, the external magnetic field \mathbf{H} has been ignored, and only an external electric field \mathbf{E} is applied to the system, while I_{e-e} is the electron-electron collision term, and is directly related to the momentum relaxation mechanism; (ii) More importantly, it has been confirmed recently that this transport equation (18) developed by Prange and Kadanoff⁶⁴ is not specific to a phonon-mediated interaction, and also is valid for the system with the interaction mediated by other bosonic excitations⁶⁵.

In the subsequent analysis, we investigate the low-temperature resistivity in the overdoped electron-doped cuprate superconductors based on the Boltzmann transport equation (18). To derive this Boltzmann transport equation (18), the linear perturbation from the equilibrium in terms of the distribution function,

$$f(\mathbf{k}) = n_{\text{F}}(\bar{\varepsilon}_{\mathbf{k}}) - \frac{dn_{\text{F}}(\bar{\varepsilon}_{\mathbf{k}})}{d\bar{\varepsilon}_{\mathbf{k}}} \tilde{\Phi}(\mathbf{k}), \quad (19)$$

can be introduced as it has been done in the previous works^{31,64,65}, where $n_{\text{F}}(\omega)$ is the fermion distribution function, $\tilde{\Phi}(\mathbf{k})$ is a local shift of the chemical potential at a given patch of EFS^{31,64,65}, and obeys the antisymmetric relation $\tilde{\Phi}(-\mathbf{k}) = -\tilde{\Phi}(\mathbf{k})$. Substituting the above result in Eq. (19) into Eq. (18), we can linearize the Boltzmann equation (18) as,

$$e\mathbf{v}_{\mathbf{k}} \cdot \mathbf{E} \frac{dn_{\text{F}}(\bar{\varepsilon}_{\mathbf{k}})}{d\bar{\varepsilon}_{\mathbf{k}}} = I_{e-e}, \quad (20)$$

with the electron velocity $\mathbf{v}_{\mathbf{k}} = \nabla_{\mathbf{k}} \bar{\epsilon}_{\mathbf{k}}$.

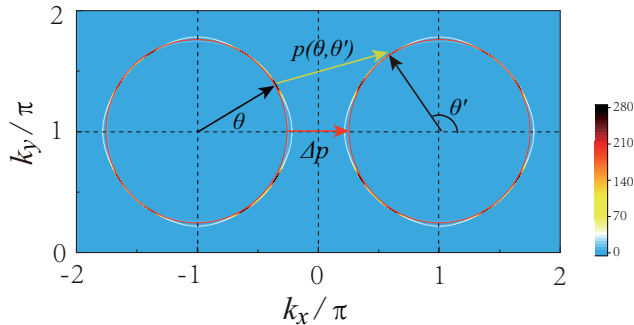


FIG. 6. (Color online) Schematic picture of the electron umklapp scattering process⁶⁵, where an electron on a electron Fermi surface (left) is scattered by its partner on the umklapp electron Fermi surface (right). The intensity map of the electron Fermi surface is the same as shown in Fig. 4, where the Fermi wave vector of the tips of the Fermi arcs k_F^{TFA} is the radius of the circular electron Fermi surface (red), and then an electron on this circular electron Fermi surface (left) parametrized by the Fermi angle θ is scattered to a point parametrized by the Fermi angle θ' on the umklapp electron Fermi surface (right) by the spin excitation carrying momentum $\mathbf{p}(\theta, \theta')$. Δ_p is the minimal umklapp vector at the antinode (the Fermi angle $\theta = 0$).

We now focus on the electron-electron collision term I_{e-e} , which is closely associated with the momentum relaxation mechanism^{25,26}. Although the momentum relaxation mechanism underlying the low-temperature T-linear resistivity in the strange metallic normal-state still remains controversial to date, it is likely of the electronic origin. In particular, it has been shown clearly that the

electron umklapp scattering plays a crucial role in the normal-state transport of cuprate superconductors^{65–67}. In this paper, we employ the electron umklapp scattering to study the low-temperature resistivity in the over-doped electron-doped cuprate superconductors. To see this electron umklapp scattering process more clearly, a schematic picture of the electron umklapp scattering process⁶⁵ is shown in Fig. 6, where an electron on a circular EFS (left) is scattered by its partner on the umklapp EFS (right). The intensity map of EFS in Fig. 6 is identical to that shown in Fig. 4, where the Fermi wave vector of the tips of the Fermi arcs k_F^{TFA} is the radius of the circular EFS (red). This circle EFS (red) connects all tips of the Fermi arcs, and then almost all the fraction of the spectral weight is located on this circular EFS.

In the recent discussions⁶⁵, it has been shown that the electrical transport in the strange metallic normal-state of the over-doped hole-doped cuprate superconductors arises from the umklapp scattering between electrons by the exchange of a critical boson propagator, where the anisotropic transport scattering rate is T-linear in the low-temperature region near the umklapp point, which induces a low-temperature T-linear resistivity. Very recently, we³¹ have also studied the nature of the electrical transport in the strange metallic normal-state of the over-doped hole-doped cuprate superconductors, where the momentum dependence of the transport scattering rate originates from the umklapp scattering between electrons by the exchange of the effective spin propagator, and scales linearly with temperature in the low-temperature region, which then naturally generates a low-temperature T-linear resistivity. Following these recent discussions^{31,65}, the electron-electron collision I_{e-e} in Eq. (20) in the present case can be derived as,

$$I_{e-e} = \frac{1}{N^2} \sum_{\mathbf{k}, \mathbf{p}} \frac{2}{T} |P(\mathbf{k}, \mathbf{p}, \mathbf{k}', \bar{\epsilon}_{\mathbf{k}} - \bar{\epsilon}_{\mathbf{k}+\mathbf{p}+\mathbf{G}})|^2 \{ \tilde{\Phi}(\mathbf{k}) + \tilde{\Phi}(\mathbf{k}') - \tilde{\Phi}(\mathbf{k} + \mathbf{p} + \mathbf{G}) - \tilde{\Phi}(\mathbf{k}' - \mathbf{p}) \} \\ \times n_F(\bar{\epsilon}_{\mathbf{k}}) n_F(\bar{\epsilon}_{\mathbf{k}'})[1 - n_F(\bar{\epsilon}_{\mathbf{k}+\mathbf{p}+\mathbf{G}})][1 - n_F(\bar{\epsilon}_{\mathbf{k}'-\mathbf{p}})] \delta(\bar{\epsilon}_{\mathbf{k}} + \bar{\epsilon}_{\mathbf{k}'} - \bar{\epsilon}_{\mathbf{k}+\mathbf{p}+\mathbf{G}} - \bar{\epsilon}_{\mathbf{k}'-\mathbf{p}}), \quad (21)$$

where \mathbf{G} labels a set of reciprocal lattice vectors, and then the above electron umklapp scattering (21) is described as a scattering between electrons by the exchange of the effective spin propagator,

$$P(\mathbf{k}, \mathbf{p}, \mathbf{k}', \omega) = \frac{1}{N} \sum_{\mathbf{q}} \Lambda_{\mathbf{p}+\mathbf{q}+\mathbf{k}} \Lambda_{\mathbf{q}+\mathbf{k}'} \Pi(\mathbf{p}, \mathbf{q}, \omega), \quad (22)$$

rather than the scattering between electrons via the emission and absorption of the spin excitation³¹.

The electron-electron collision I_{e-e} in Eq. (21) are both functions of momentum and energy, where the magnitude of wave vector dependence is unimportant at low temperatures, since everything happens at EFS^{25,26,64–68}. In this case, a given patch at the circular

EFS shown in Fig. 6 is depicted via the Fermi angle θ with the angle range $\theta \in [0, 2\pi]$, which leads to that the momentum integration along the perpendicular momentum is replaced by the integration over $\bar{\epsilon}_{\mathbf{k}}$ ^{64,65}. In the present case of the umklapp scattering between electrons by the exchange of the effective spin propagator, an electron on the circular EFS parametrized by the Fermi angle θ is scattered to a point parametrized by the Fermi angle θ' on the umklapp EFS in terms of the spin excitation carrying momentum $\mathbf{p}(\theta, \theta')$ as shown in Fig. 6. With the help of the above treatment, the electron-electron collision I_{e-e} in Eq. (21) can be derived straightforwardly, and has been given explicitly in Ref. 31. In this case, the

Boltzmann transport equation (20) can be obtained as,

$$e\mathbf{v}_F(\theta) \cdot \mathbf{E} = -2 \int \frac{d\theta'}{2\pi} \zeta(\theta') F(\theta, \theta') [\Phi(\theta) - \Phi(\theta')], \quad (23)$$

with $\Phi(\theta) = \tilde{\Phi}[\mathbf{k}(\theta)]$, the Fermi velocity $\mathbf{v}_F(\theta)$ at the Fermi angle θ , the density of states factor $\zeta(\theta') = k_F^2/[4\pi^2 v_F^3]$ at angle θ' , the Fermi wave vector k_F , and the Fermi velocity v_F . In this case, the antisymmetric relation $\tilde{\Phi}(-\mathbf{k}) = -\tilde{\Phi}(\mathbf{k})$ for $\tilde{\Phi}(\mathbf{k})$ in Eq. (19) is replaced by the antisymmetric relation $\Phi(\theta) = -\Phi(\theta + \pi)$ for $\Phi(\theta)$ in the above Eq. (23). Moreover, the coefficient of $\Phi(\theta)$ in the first term of the right-hand side of Eq. (23),

$$\gamma(\theta) = 2 \int \frac{d\theta'}{2\pi} \zeta(\theta') F(\theta, \theta'), \quad (24)$$

is identified as the angular dependence of the transport scattering rate^{31,65}, where as shown in Fig. 6, the kernel function $F(\theta, \theta')$ links up the point θ on the circular EFS with the point θ' on the umklapp EFS via the magnitude of the momentum transfer $p(\theta, \theta')$, and can be expressed explicitly as,

$$F(\theta, \theta') = \frac{1}{T} \int \frac{d\omega}{2\pi} \frac{\omega^2}{p(\theta, \theta')} |\bar{P}[\mathbf{k}(\theta), p(\theta, \theta'), \omega]|^2 \times n_B(\omega)[1 + n_B(\omega)], \quad (25)$$

where the reduced effective spin propagator $\bar{P}[\mathbf{k}(\theta), p(\theta, \theta'), \omega]$ has been given explicitly in Ref.³¹.

III. SCALING OF LOW-TEMPERATURE TRANSPORT SCATTERING

The electron current density now can be derived via the local shift of the chemical potential $\Phi(\theta)$ as³¹,

$$\begin{aligned} \mathbf{J} &= en_0 \frac{1}{N} \sum_{\mathbf{k}} \mathbf{v}_{\mathbf{k}} \frac{dn_F(\bar{\epsilon}_{\mathbf{k}})}{d\bar{\epsilon}_{\mathbf{k}}} \tilde{\Phi}(\mathbf{k}) \\ &= -en_0 \frac{k_F}{v_F} \int \frac{d\theta}{(2\pi)^2} \mathbf{v}_F(\theta) \Phi(\theta), \end{aligned} \quad (26)$$

where the momentum relaxation is induced by the action of the electric field on the mobile electrons at EFS with the density n_0 . In particular, the local shift of the chemical potential $\Phi(\theta)$ can be obtained in the relaxation-time approximation as^{31,65}, $\Phi(\theta) = -ev_F \cos(\theta) E_{\hat{x}}/[2\gamma(\theta)]$, with the electric field \mathbf{E} that has been chosen along the \hat{x} -axis. In this case, the dc conductivity can be obtained straightforwardly as^{31,65},

$$\sigma_{dc}(T) = \frac{1}{2} e^2 n_0 k_F v_F \int \frac{d\theta}{(2\pi)^2} \cos^2(\theta) \frac{1}{\gamma(\theta)}, \quad (27)$$

while the resistivity is related directly to the above dc conductivity, and can be expressed explicitly as,

$$\rho(T) = \frac{1}{\sigma_{dc}(T)}. \quad (28)$$

The above results therefore show that the electron-electron collision I_{e-e} (21) originated from the umklapp scattering between electrons by the exchange of the effective spin propagator leads to the appearance of the electrical resistance.

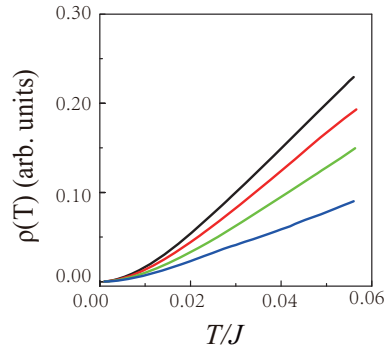


FIG. 7. (Color online) The resistivity as a function of temperature at $\delta = 0.15$ (black-line), $\delta = 0.17$ (red-line), $\delta = 0.19$ (green-line), and $\delta = 0.21$ (blue-line).

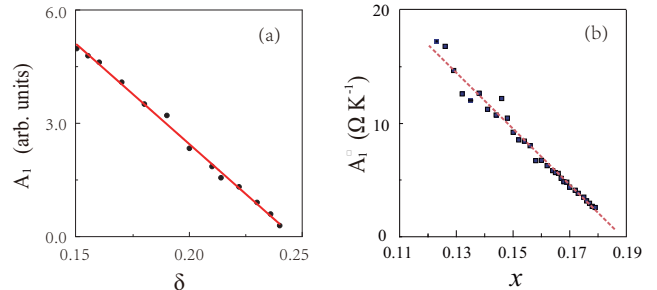


FIG. 8. (a) The strength of the low-temperature T-linear resistivity (black dots) as a function of doping. (b) The corresponding experimental result of $\text{La}_{2-x}\text{Ce}_x\text{CuO}_4$ taken from Ref. 23.

Now we are ready to discuss the exotic properties of the low-temperature resistivity in the overdoped electron-doped cuprate superconductors. In Fig. 7, we plot the resistivity $\rho(T)$ in Eq. (28) as a function of temperature at the electron doping concentrations $\delta = 0.15$ (black-line), $\delta = 0.17$ (red-line), $\delta = 0.19$ (green-line), and $\delta = 0.21$ (blue-line), where the temperature region is clearly divided into two characteristic regions: (i) the low-temperature region ($T > 0.01J \approx 10\text{K}$), where the resistivity $\rho(T)$ is T-linear over a wide range of the electron doping in the overdoped regime, with the strength of the T-linear resistivity (then the T-linear resistivity coefficient) A_1 that decreases with the increase of the electron doping all the way up to the edge of the SC dome, in qualitative agreement with the corresponding experimental results¹⁷⁻²³. To see this evolution of the T-linear resistivity strength A_1 with the electron doping more clearly, we plot A_1 as a function of the electron doping in Fig. 8a, where the data (black dots) are the numerical results from Eq. (28), while the red-line is guide

for the eyes. For a better comparison, the corresponding experimental result²³ observed on the electron-doped cuprate superconductor $\text{La}_{2-x}\text{Ce}_x\text{CuO}_4$ in the overdoped regime is also shown in Fig. 8b. The obtained result in Fig. 8a thus shows that A_1 almost linearly *decreases* with the increase of the electron doping concentration for the overdoping up to the edge of the SC dome, also in qualitative agreement with the corresponding experimental data^{17–23}; (ii) the far-lower-temperature region ($T < 0.01J \approx 10\text{K}$), where the resistivity $\rho(T)$ is nonlinear in temperature. To see this nonlinear behaviour more clearly, we have fitted the present result of the resistivity $\rho(T)$ in the far-lower-temperature region, and found that in the far-lower-temperature region, the resistivity decreases quadratically with the decrease of temperature.

The low-temperature T-linear resistivity occurring in the overdoped electron-doped cuprate superconductors^{17–23} has been also detected experimentally in the overdoped hole-doped cuprate superconductors^{69–72}, indicating that the low-temperature T-linear resistivity is a generic feature in the strange-metal phase of both the overdoped electron- and hole-doped cuprate superconductors. These experimental observations^{17–23,69–72} show the same physical origin of the low-temperature T-linear resistivity in both the overdoped electron- and hole-doped cuprate superconductors. In this case, we³¹ have also investigated the low-temperature T-linear resistivity in the overdoped hole-doped cuprate superconductors, and the results show that as in the present case of the low-temperature T-linear resistivity in the electron-doped cuprate superconductors, the mechanism of the momentum relaxation for the low-temperature T-linear resistivity in the overdoped hole-doped cuprate superconductors originates from the same umklapp scattering between electrons by the exchange of the effective spin propagator.

In addition to the above results of the low-temperature T-linear resistivity, we have also performed a numerical calculation for the transport scattering rate $\gamma(\theta)$ in Eq. (24), and the obtained results show that the overall feature of the strong angular dependence of $\gamma(\theta)$ in the electron-doped side is quite similar to the corresponding one in the hole-doped case³¹, where $\gamma(\theta)$ has the largest value at around the antinodal region, and then it decreases with the move of the Fermi angle away from the antinode. In particular, although the magnitude of $\gamma(\theta)$ at around the nodal region is smaller than that at around the antinodal region, $\gamma(\theta)$ exhibits its minimum at around the tips of the Fermi arcs, which therefore show that the normal-state transport is mainly governed by $\gamma(\theta)$ at the antinodal region. This also follows a fact that as in the hole-doped case³¹, the characteristic feature of the tips of the Fermi arcs shown in Fig. 4 is that both the real and imaginary parts of the electron normal self-energy have the anomalously small values^{30,57}, indicating that the interaction (then the scattering) between electrons at around the tips of the Fermi arcs is particu-

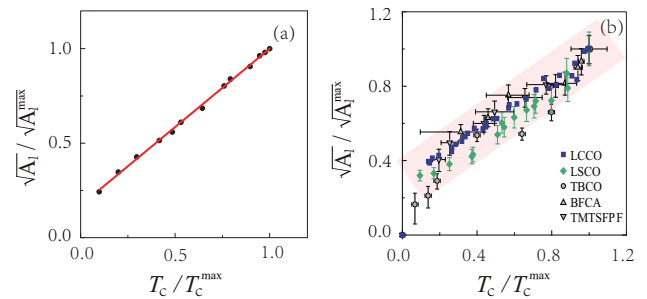


FIG. 9. (a) The correlation (black dots) between the square-root of the T-linear resistivity strength $\sqrt{A_1}/\sqrt{A_1^{\max}}$ and the corresponding magnitude of T_c/T_c^{\max} , where A_1^{\max} and T_c^{\max} are maximal values of the T-linear resistivity strength and superconducting transition temperature at the optimal electron doping, respectively. (b) The experimental results taken from Ref. 23, where the squares are the data from $\text{La}_{2-x}\text{Ce}_x\text{CuO}_4$, the diamonds are the data from $\text{La}_{2-x}\text{Sr}_x\text{CuO}_4$, the circles are the data from $\text{Tl}_2\text{Ba}_2\text{CuO}_{6+\delta}$, the upper triangles are the data from $\text{Ba}(\text{Fe}_{1-x}\text{Co}_x)_2\text{As}_2$, and the lower triangles are the data from $(\text{TMTSF})_2\text{PF}_6$.

larly weak. In other words, although the electron density of states is largest at around the tips of the Fermi arcs, the electron scattering at around the tips of the Fermi arcs is quite weak, and then the electrons at around the tips of the Fermi arcs move more freely than those at other parts of EFS. The current results together with our recent work for the hole-doped case³¹ therefore also show that the electron umklapp scattering from the spin excitation can give a consistent description of the low-temperature T-linear resistivity in both the overdoped hole- and electron-doped cuprate superconductors.

We now turn to discuss the intrinsic correlation between the strength of the low-temperature T-linear resistivity and the corresponding magnitude of T_c in the overdoped electron-doped cuprate superconductors. In Fig. 9a, we plot the square-root of the strength of the low-temperature T-linear resistivity $\sqrt{A_1}$ as a function of T_c . The theoretical results (black dots) in Fig. 9a are extracted from the data in Fig. 3a and Fig. 8a, while the red-line is guide for the eyes. For a clear comparison, the corresponding experimental result²³ observed on $\text{La}_{2-x}\text{Ce}_x\text{CuO}_4$ in the overdoped regime is also shown in Fig. 9b (the squares). It thus shows clearly in Fig. 9 that the experimental result²³ of the scaling relation between the strength of the low-temperature T-linear resistivity $\sqrt{A_1}$ and the corresponding magnitude of T_c in the overdoped electron-doped cuprate superconductors is qualitatively reproduced. $\sqrt{A_1}/\sqrt{A_1^{\max}}$ is grown linearly when T_c/T_c^{\max} is raised, with A_1^{\max} and T_c^{\max} that are maximal values of the strength of the T-linear resistivity and SC transition temperature at the optimal electron doping, respectively. In other words, the evolution of T_c correlates with the emergence of the low-temperature T-linear resistivity in the overdoped regime, and then the magnitude of $\sqrt{A_1}$ decreases as T_c decreases. The

present result of the scaling relation in Fig. 9 therefore also confirms the intimate connection between the nature of the strange metallic normal-state and superconductivity observed on the overdoped electron-doped cuprate superconductors^{17–23}. It should be noted that this correlation between the strength of the low-temperature T-linear resistivity and the corresponding magnitude of T_c may be a universal feature of not only the cuprate superconductors but also many other unconventional superconductors, since as the experimental data²³ shown in Fig. 9b, the correlation between the strength of the low-temperature T-linear resistivity and the corresponding magnitude of T_c has been observed experimentally on the overdoped hole-doped cuprate superconductors^{13,23,73}, such as $\text{La}_{2-x}\text{Sr}_x\text{CuO}_4$ (the diamonds in Fig. 9b) and $\text{Tl}_2\text{Ba}_2\text{CuO}_{6+\delta}$ (the circles in Fig. 9b), and many other unconventional superconductors^{13,23,74}, such as the single-band organic superconductor $(\text{TMTSF})_2\text{PF}_6$ (the lower triangles in Fig. 9b) as well as the iron-based superconductor $\text{Ba}(\text{Fe}_{1-x}\text{Co}_x)_2\text{As}_2$ (the upper triangulars in Fig. 9b).

The essential physics of the crossover from the T-linear resistivity in the low-temperature region into T-quadratic resistivity in the far-lower-temperature region invoked for the overdoped hole-doped case³¹ straightforwardly applies here on the overdoped electron-doped side, and is attributed to the electron umklapp scattering mediated by the spin excitation. The nature of the transport scattering rate in Eq. (24) [then the nature of the resistivity in Eq. (28)] is dominated by the nature of the kernel function $F(\theta, \theta')$ in Eq. (25). However, this kernel function $F(\theta, \theta')$ is proportional to the effective spin propagator $P(\mathbf{k}, \mathbf{p}, \mathbf{k}', \omega)$ in Eq. (22), which can be expressed more clearly as,

$$P(\mathbf{k}, \mathbf{p}, \mathbf{k}', \omega) = -\frac{1}{N} \sum_{\mathbf{q}} \left[\frac{\varpi_1(\mathbf{k}, \mathbf{p}, \mathbf{k}', \mathbf{q})}{\omega^2 - [\omega_{\mathbf{p}\mathbf{q}}^{(1)}]^2} - \frac{\varpi_2(\mathbf{k}, \mathbf{p}, \mathbf{k}', \mathbf{q})}{\omega^2 - [\omega_{\mathbf{p}\mathbf{q}}^{(2)}]^2} \right], \quad (29)$$

with the functions,

$$\varpi_1(\mathbf{k}, \mathbf{p}, \mathbf{k}', \mathbf{q}) = \Lambda_{\mathbf{k}+\mathbf{p}+\mathbf{q}} \Lambda_{\mathbf{q}+\mathbf{k}'} \bar{W}_{\mathbf{p}\mathbf{q}}^{(1)}, \quad (30a)$$

$$\varpi_2(\mathbf{k}, \mathbf{p}, \mathbf{k}', \mathbf{q}) = \Lambda_{\mathbf{k}+\mathbf{p}+\mathbf{q}} \Lambda_{\mathbf{q}+\mathbf{k}'} \bar{W}_{\mathbf{p}\mathbf{q}}^{(2)}. \quad (30b)$$

Following the recent discussions for the hole-doped case³¹, we can also make a Taylor expansion for the effective spin excitation energy dispersions $\omega_{\mathbf{p}\mathbf{q}}^{(1)}$ and $\omega_{\mathbf{p}\mathbf{q}}^{(2)}$ in the electron-doped side, and then the effective spin excitation energy dispersions $\omega_{\mathbf{p}\mathbf{q}}^{(1)}$ and $\omega_{\mathbf{p}\mathbf{q}}^{(2)}$ can be obtained approximately as,

$$\omega_{\mathbf{p}\mathbf{q}}^{(1)} = \omega_{\mathbf{q}+\mathbf{p}} + \omega_{\mathbf{q}} \approx a(\mathbf{q})p^2 + 2\omega_{\mathbf{q}}, \quad (31a)$$

$$\omega_{\mathbf{p}\mathbf{q}}^{(2)} = \omega_{\mathbf{q}+\mathbf{p}} - \omega_{\mathbf{q}} \approx a(\mathbf{q})p^2, \quad (31b)$$

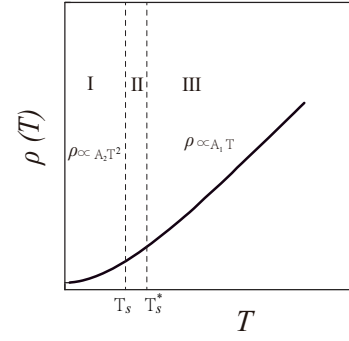


FIG. 10. Schematic regions of the low-temperature resistivity in the overdoped electron-doped cuprate superconductors, where $T_s^* = T_{\text{scale}} + \omega_{\mathbf{k}_A}$, $\omega_{\mathbf{k}_A}$ is the spin excitation energy at the $[\pi, \pi]$ point of the Brillouin zone, and $T_s = T_{\text{scale}}$. (I) The far-lower-temperature region ($T < T_s$), where the resistivity decreases quadratically as the temperature decreases; (II) The extremely-narrow-crossover region ($T_s < T < T_s^*$), where the resistivity is neither T-linear nor T-quadratic, but is a nonlinear in temperature; (III) The low-temperature region ($T > T_s^*$), where the resistivity is T-linear.

with $a(\mathbf{q}) = (d^2\omega_{\mathbf{q}}/d^2\mathbf{q})$. The above results in Eq. (31) show that the effective spin propagator $P(\mathbf{k}, \mathbf{p}, \mathbf{k}', \omega)$ in Eq. (29) scales with p^2 . Moreover, when the electron umklapp scattering kicks in, the temperature scale that is proportional to Δ_p^2 can be very low^{31,65} due to the presence of this p^2 scaling in the effective spin propagator (29). In this case, $T_{\text{scale}} = \bar{a}\Delta_p^2$ can be identified as the temperature scale, with the average value $\bar{a} = (1/N) \sum_{\mathbf{q}} a(\mathbf{q})$ that is a constant at a given electron doping. In particular, our numerical result indicates that the temperature scale $T_{\text{scale}} = \bar{a}\Delta_p^2 = 0.01247J \approx 12\text{K}$ at the electron doping concentration $\delta = 0.19$, also in good agreement with the crossover temperature shown in Fig. 7.

According to the above temperature scale T_{scale} , we now follows the analyses carried out in the hole-doped case³¹ to show that the temperature region in the electron-doped side shown in Fig. 7 can also be divided into three characteristic regions:

(i) the low-temperature region, where $T > T_{\text{scale}} + \omega_{\mathbf{k}_A}$ with the spin excitation energy $\omega_{\mathbf{k}_A} \approx 0.0022J \sim 2\text{K}$ at the $[\pi, \pi]$ point of BZ. In this low-temperature region, the kernel function $F(\theta, \theta')$ can be reduced as $F(\theta, \theta') \propto T$, which generates a low-temperature T-linear resistivity $\rho(T) \propto T$ as shown in Fig. 7;

(ii) the far-lower-temperature region, where $T < T_{\text{scale}}$. In this far-lower-temperature region, the kernel function $F(\theta, \theta')$ can be reduced as $F(\theta, \theta') \propto T^2$, which leads to a T-quadratic resistivity $\rho(T) \propto T^2$ as shown in Fig. 7;

(iii) the crossover temperature region, where $T_{\text{scale}} < T < T_{\text{scale}} + \omega_{\mathbf{k}_A}$. In this extremely-narrow-crossover temperature region, the resistivity does not exhibit a T-linear or a T-quadratic behavior, but instead shows a nonlinear behavior with respect to temperature. The above three

characteristic regions can be summarized schematically in Fig. 10, where $T_s^* = T_{\text{scale}} + \omega_{\mathbf{k}_A}$, and $T_s = T_{\text{scale}}$.

We now turn to show why the strength of the low-temperature T-linear resistivity correlates with the corresponding magnitude of T_c in the overdoped electron-doped cuprate superconductors to form the scaling relation shown Fig. 9: (i) in the framework of the kinetic-energy-driven superconductivity⁴⁰⁻⁴³, the main ingredient is identified into an electron pairing mechanism involving *the spin excitation*, where both the electron pair gap (then the anomalous self-energy in the particle-particle channel) and the single-particle coherence (then the normal self-energy in the particle-hole channel) arise from the interaction between electrons mediated by *the spin excitation*. In this case, the SC-state is controlled by both the electron pair gap and the single-particle coherence, which leads to that the maximal T_c occurs around the optimal electron doping, and then decreases in both the underdoped and the overdoped regimes as shown in Fig. 3; (ii) on the other hand, the results presented here show that the low-temperature T-linear resistivity in the overdoped regime shown in Fig. 7 arises from the momentum relaxation due to the electron umklapp scattering mediated by *the same spin excitation*, and then the strength of the low-temperature T-linear resistivity decreases as T_c decreases as shown in Fig. 8. In other words, this *same spin excitation* that mediates both the pairing electrons responsible for superconductivity and the electron umklapp scattering responsible for the low-temperature T-linear resistivity induces a correlation between the strength of the low-temperature T-linear resistivity and the corresponding magnitude of T_c in the overdoped electron-doped cuprate superconductors as shown in Fig. 9.

Superconductivity in the electron-doped cuprate superconductors with the highest T_c emerges directly as an instability of the strange metallic normal-state⁸⁻¹¹, where the electronic state exhibits the non-Fermi-liquid behaviour. It was realized that the fundamental principles must be involved in the understanding of the overdoped strange-metal regime²⁷⁻²⁹. However, if we look more closely at cuprate superconductors, then there is a lot of evidences in favour of the t - J model as the basic underlying microscopic model⁷⁵. More specifically, the ARPES experimental observations^{34,51-53} indicate that the t - J model (1) is of particular relevance to the low energy features of cuprate superconductors. In this case, the non-Fermi-liquid behaviour of cuprate superconductors have been studied based directly on the t - J model^{32-34,38,49,76-83}, where it has been shown that the non-Fermi-liquid behaviour is due to strong electron scattering mediated by the spin fluctuations. Starting from the t - J model (1), we^{30,46,57} have also studied recently the intrinsic features of the electronic structure of the electron-doped cuprate superconductors, where the coupling of a spin excitation to electron quasiparticles leads to the emergence of the peak-dip-hump structure in the quasiparticle excitation spectrum and the kink

in the quasiparticle dispersion, in agreement with the corresponding experimental data⁸⁻¹¹. These results of the low-energy electronic structure^{30,46,57} together with the present results of the low-temperature T-linear resistivity in the overdoped regime show that the same spin excitation that is responsible for pairing the electrons also dominantly scatters the electrons in the overdoped strange-metal phase responsible for the low-energy electronic structure. All these results^{30,32-34,38,46,57,76-83} therefore indicates that the strong scattering between electrons mediated by the spin excitations plays a crucial role in the understanding of the non-Fermi-liquid behaviour in the overdoped electron-doped cuprate superconductors.

IV. SUMMARY

Within the framework of the kinetic-energy-driven superconductivity, we have rederived the doping dependence of T_c in the electron-doped cuprate superconductors, where the glue to hold the constrained electron pairs together is *the spin excitation, the collective mode from the internal spin degree of freedom of the constrained electron itself*, then T_c achieves its maximum at around the optimal electron doping, and decreases in both the underdoped and overdoped regimes. By virtue of this doping dependence of T_c , we then have investigated the correlation between the strength of the low-temperature T-linear resistivity and the corresponding magnitude of T_c in the overdoped electron-doped cuprate superconductors, where the low-temperature T-linear resistivity in the overdoped regime arises from the momentum relaxation due to the electron umklapp scattering mediated by *the same spin excitation*. The result of the low-temperature T-linear resistivity in this paper together with the previous work for superconductivity³⁰ therefore identify explicitly a fact: *the spin excitation* that acts like a bosonic glue to hold the electron pairs together responsible for superconductivity also mediates the electron umklapp scattering responsible for the low-temperature T-linear resistivity in the overdoped regime. This *same spin excitation* therefore leads to that the strength of the low-temperature T-linear resistivity well tracks the corresponding magnitude of T_c in the overdoped electron-doped cuprate superconductors.

After intensive investigations about four decades, although the underlying scattering mechanism for the low-temperature resistivity of cuprate superconductors still remains controversial, the electron umklapp scattering is believed to be at the heart of the exotic features of the low-temperature resistivity in cuprate superconductors^{31,65-67}. In particular, it has been shown that the low-temperature T-linear resistivity in the overdoped strange-metal phase originates from the electron umklapp scattering⁶⁵. On the other hand, it has been shown that the electron umklapp scattering processes, which directly transfer momentum between the electron

sea and the underlying square lattice, lead to the T-linear resistivity in the strange-metal phase⁶⁶. More specifically, the momentum relaxation due to the electron umklapp scattering mediated by the spin excitations has been employed recently to study the nature of the low-temperature T-linear resistivity in the overdoped strange-metal phase³¹, where the underlying scattering rate is T-linear near the umklapp point, which therefore leads to a low-temperature T-linear resistivity. All the results obtained from these studies^{31,65–67} are well consistent with the corresponding experimental observations, and therefore confirm that the low-temperature T-linear resistivity in the strange-metal phase^{17–23,69–72} arises from the electron umklapp scattering.

Finally, it should be noted that the effective spin propagator $P(\mathbf{k}, \mathbf{p}, \mathbf{k}', \omega)$ in Eq. (22) is obtained in the mean-field (MF) level⁴⁸, i.e., $P(\mathbf{k}, \mathbf{p}, \mathbf{k}', \omega)$ in Eq. (22) is obtained in terms of the convolution of two MF spin propagators in Eq. (10). In this case, the umklapp scattering between electrons in Eq. (21) by the exchange of the effective MF spin propagator is better suited for the interpretation of the low-temperature T-linear resistivity in the strange-metal phase of the overdoped electron-doped cuprate superconductors, as it has been done for the case in the overdoped hole-doped cuprate superconductors³¹. This follows a basic fact that as the results shown in Refs. 40 and 42, the coupling strength of the electrons with the spin excitations gradually weakens with the increase of doping from a strong-coupling case in the underdoped regime to a weak-coupling side in the overdoped regime^{13,84–86}, reflecting a reduction of the strength of the AF fluctuation with the increase of doping. In other words, the effect of the AF fluctuation in the overdoped regime is less dramatic than in the underdoped regime^{13,87–89}, leading to that the AF (then the normal-state) pseudogap effect created by the AF fluctuation is quite weak^{8,45,90}. However, in the underdoped regime, the effect of the AF fluctuation is much dramatic^{13,87–89}, and can be described in terms of the full spin propagator⁴⁸, where the spin self-energy is derived in terms of the charge-carrier bubble. In particular, the AF (then the normal-state) pseudogap effect generated by the dramatic AF fluctuation in the underdoped regime is quite strong^{8,45,90}, and then this pseudogap lowers the density of the spin excitations in response to the electron umklapp scattering. In this case, the electron umklapp scattering should be mediated by the exchange of the effective full spin propagator for a proper description of the low-temperature resistivity in the underdoped electron-doped cuprate superconductors. These and the related issues are under investigation now. In particular, the low-temperature T-quadratic resistivity of the underdoped hole-doped cuprate superconductors has been discussed very recently⁹¹, where the scattering rate arises from the electron umklapp scattering by the exchange of the effective full spin propagator. The obtained results of the low-temperature T-quadratic resistivity in the underdoped regime⁹¹ together with the study on the low-temperature

T-linear resistivity in the overdoped regime³¹ show that the the electron umklapp scattering from a spin excitation responsible for the low-temperature T-linear resistivity in the overdoped regime naturally produces the low-temperature T-quadratic resistivity in the underdoped regime resulting from the opening of a momentum dependent spin pseudogap. This underlying mechanism of the electron umklapp scattering from a spin excitation^{31,91} is also confirmed from the experimental analyses^{92–96}, where it has been shown that if the electron scattering responsible for the low-temperature T-linear resistivity in the overdoped regime involves the electron scattering on the spin excitations in the underdoped regime, then the spin pseudogap seen in nuclear magnetic resonance and nuclear quadrupole resonance below the normal-state pseudogap crossover temperature would naturally account for a deviation from the low-temperature T-linear behaviour of the resistivity. Since the common scattering mechanism linking the low-temperature resistivity of both the hole- and electron-doped cuprate superconductors, the present theory also predicts that the variation of the low-temperature resistivity in the underdoped electron-doped cuprate superconductors deviates from the T-linear behaviour, while this deviation from the low-temperature T-linear behaviour of the resistivity has been observed experimentally in the underdoped electron-doped cuprate superconductors^{16–21}.

ACKNOWLEDGEMENTS

X. Ma would like to thank Faculty of Arts and Sciences, Beijing Normal University at Zhuhai for the hospitality.

DISCLOSURE STATEMENT

No potential conflict of interest was reported by the authors.

FUNDING

XM, MZ, and SP are supported by the National Key Research and Development Program of China under Grant Nos. 2023YFA1406500 and 2021YFA1401803, and the National Natural Science Foundation of China under Grant Nos. 12274036 and 12247116. HG acknowledges support from the National Natural Science Foundation of China under Grant Nos. 11774019 and 12074022.

Appendix A: Derivation of superconducting transition temperature T_c

In this Appendix, our main goal is to generalize the theoretical framework of the kinetic-energy-driven superconductivity from the previous hole-doped case^{39–43} to

the present electron-doped case, and then derive the full hole diagonal and off-diagonal propagators $G_f(\mathbf{k}, \omega)$ and $\mathfrak{S}_f^\dagger(\mathbf{k}, \omega)$ in Eq. (5) of the main text.

1. Mean-field theory

In the MF level, the t - J model (4) in the main text can be decoupled as,

$$H_{\text{MF}} = H_t + H_J + H_0, \quad (\text{A1a})$$

$$H_t = -\chi_1 t \sum_{\langle ll' \rangle \sigma} a_{l'\sigma}^\dagger a_{l\sigma} + \chi_2 t' \sum_{\langle\langle ll' \rangle\rangle \sigma} a_{l'\sigma}^\dagger a_{l\sigma} + \mu_a \sum_{l\sigma} a_{l\sigma}^\dagger a_{l\sigma}, \quad (\text{A1b})$$

$$H_J = \frac{1}{2} J_{\text{eff}} \sum_{\langle ll' \rangle} [\epsilon(S_l^+ S_{l'}^- + S_l^- S_{l'}^+) + 2S_l^z S_{l'}^z] + t' \phi_2 \sum_{\langle\langle ll' \rangle\rangle} (S_l^+ S_{l'}^- + S_l^- S_{l'}^+), \quad (\text{A1c})$$

where $H_0 = 8Nt\phi_1\chi_1 - 8Nt'\phi_2\chi_2$, $\epsilon = 1 - 2t\phi_1/J_{\text{eff}}$, the charge-carrier's particle-hole parameters $\phi_1 = \langle a_{l\sigma}^\dagger a_{l+\hat{\eta}\sigma} \rangle$ and $\phi_2 = \langle a_{l\sigma}^\dagger a_{l+\hat{\tau}\sigma} \rangle$, and the spin correlation functions $\chi_1 = \langle S_l^+ S_{l+\hat{\eta}}^- \rangle$ and $\chi_2 = \langle S_l^+ S_{l+\hat{\tau}}^- \rangle$, with $\hat{\eta} = \hat{x}$, \hat{y} and $\hat{\tau} = \hat{x} \pm \hat{y}$.

According to the above charge-carrier part (A1b), the MF charge-carrier propagator can be obtained straightforwardly as,

$$g_a^{(0)}(\mathbf{k}, \omega) = \frac{1}{\omega - \xi_{\mathbf{k}}^{(a)}}, \quad (\text{A2})$$

with the MF charge-carrier band energy,

$$\xi_{\mathbf{k}}^{(a)} = -4\chi_1 t \gamma_{\mathbf{k}} + 4t' \chi_2 \gamma'_{\mathbf{k}} + \mu_a. \quad (\text{A3})$$

On the other hand, in the doped regime without AFLRO, i.e., $\langle S_l^z \rangle = 0$, the spin propagator can be evaluated within the Kondo-Yamaji decoupling scheme⁹⁷, which is a stage one-step further than the Tyablikov's decoupling scheme⁹⁸. In particular, in the MF level, the spin part in Eq. (A1c) is described by an anisotropic Heisenberg model. In this case, two spin propagators $D(l-l', t-t') = -i\theta(t-t') \langle [S_l^+(t), S_{l'}^-(t')] \rangle = \langle \langle S_l^+(t); S_{l'}^-(t') \rangle \rangle$ and $D_z(l-l', t-t') = -i\theta(t-t') \langle [S_l^z(t), S_{l'}^z(t')] \rangle = \langle \langle S_l^z(t); S_{l'}^z(t') \rangle \rangle$ are needed to give a proper description of the nature of the spin excitation⁴⁸. Following these previous discussions⁴⁸, the spin propagators $D^{(0)}(\mathbf{k}, \omega)$ and $D_z^{(0)}(\mathbf{k}, \omega)$ can be respectively obtained as,

$$D^{(0)}(\mathbf{k}, \omega) = \frac{B_{\mathbf{k}}}{2\omega_{\mathbf{k}}} \left(\frac{1}{\omega - \omega_{\mathbf{k}}} - \frac{1}{\omega + \omega_{\mathbf{k}}} \right), \quad (\text{A4a})$$

$$D_z^{(0)}(\mathbf{k}, \omega) = \frac{B_{z\mathbf{k}}}{2\omega_{z\mathbf{k}}} \left(\frac{1}{\omega - \omega_{z\mathbf{k}}} - \frac{1}{\omega + \omega_{z\mathbf{k}}} \right), \quad (\text{A4b})$$

as quoted in Eq. (10) of the main text, with the weight functions,

$$B_{\mathbf{k}} = \lambda_1 [2\chi_1^z (\epsilon \gamma_{\mathbf{k}} - 1) + \chi_1 (\gamma_{\mathbf{k}} - \epsilon)] - \lambda_2 (2\chi_2^z \gamma'_{\mathbf{k}} - \chi_2), \quad (\text{A5a})$$

$$B_{z\mathbf{k}} = \epsilon \chi_1 \lambda_1 (\gamma_{\mathbf{k}} - 1) - \chi_2 \lambda_2 (\gamma'_{\mathbf{k}} - 1), \quad (\text{A5b})$$

respectively, while the spin excitation spectra $\omega_{\mathbf{k}}$ and $\omega_{z\mathbf{k}}$ that are given by,

$$\omega_{\mathbf{k}}^2 = \lambda_1^2 \left[\frac{1}{2} \epsilon \left(A_1 - \frac{1}{2} \alpha \chi_1^z - \alpha \chi_1 \gamma_{\mathbf{k}} \right) (\epsilon - \gamma_{\mathbf{k}}) + \left(A_2 - \frac{1}{2Z} \alpha \epsilon \chi_1 - \alpha \epsilon \chi_1^z \gamma_{\mathbf{k}} \right) (1 - \epsilon \gamma_{\mathbf{k}}) \right] + \lambda_2^2 \left[\alpha \left(\chi_2^z \gamma'_{\mathbf{k}} - \frac{3}{2Z} \chi_2 \right) \gamma'_{\mathbf{k}} + \frac{1}{2} \left(A_3 - \frac{1}{2} \alpha \chi_2^z \right) \right] + \lambda_1 \lambda_2 \left[\alpha \chi_1^z (1 - \epsilon \gamma_{\mathbf{k}}) \gamma'_{\mathbf{k}} + \frac{1}{2} \alpha (\chi_1 \gamma'_{\mathbf{k}} - C_3) (\epsilon - \gamma_{\mathbf{k}}) \right] + \alpha \gamma'_{\mathbf{k}} (C_3^z - \epsilon \chi_2^z \gamma_{\mathbf{k}}) - \frac{1}{2} \alpha \epsilon (C_3 - \chi_2 \gamma_{\mathbf{k}}), \quad (\text{A6a})$$

$$\omega_{z\mathbf{k}}^2 = \epsilon \lambda_1^2 \left(\epsilon A_1 - \frac{1}{Z} \alpha \chi_1 - \alpha \chi_1 \gamma_{\mathbf{k}} \right) (1 - \gamma_{\mathbf{k}}) + \lambda_2^2 A_3 (1 - \gamma'_{\mathbf{k}}) + \lambda_1 \lambda_2 [\alpha \epsilon C_3 (\gamma_{\mathbf{k}} - 1) + \alpha (\chi_2 \gamma_{\mathbf{k}} - \epsilon C_3) (1 - \gamma'_{\mathbf{k}})], \quad (\text{A6b})$$

respectively, where $\lambda_1 = 2ZJ_{\text{eff}}$, $\lambda_2 = 4Z\phi_2 t'$, $A_1 = \alpha C_1 + (1 - \alpha)/(2Z)$, $A_2 = \alpha C_1^z + (1 - \alpha)/(4Z)$, $A_3 = \alpha C_2 + (1 - \alpha)/(2Z)$, the spin correlation functions $\chi_1^z = \langle S_l^z S_{l+\hat{\eta}}^z \rangle$, $\chi_2^z = \langle S_l^z S_{l+\hat{\tau}}^z \rangle$, $C_1 = (1/Z^2) \sum_{\hat{\eta}, \hat{\eta}'} \langle S_{l+\hat{\eta}}^+ S_{l+\hat{\eta}'}^- \rangle$, $C_1^z = (1/Z^2) \sum_{\hat{\eta}, \hat{\eta}'} \langle S_{l+\hat{\eta}}^z S_{l+\hat{\eta}'}^z \rangle$, $C_2 = (1/Z^2) \sum_{\hat{\tau}, \hat{\tau}'} \langle S_{l+\hat{\tau}}^+ S_{l+\hat{\tau}'}^- \rangle$, $C_3 = (1/Z) \sum_{\hat{\tau}} \langle S_{l+\hat{\eta}}^+ S_{l+\hat{\tau}}^- \rangle$, $C_3^z = (1/Z) \sum_{\hat{\tau}} \langle S_{l+\hat{\eta}}^z S_{l+\hat{\tau}}^z \rangle$, and $Z = 4$ is the number of the NN or next NN sites. In order to fulfill the sum rule of the correlation function $\langle S_l^+ S_l^- \rangle = 1/2$ in the case without an AFLRO, the important decoupling parameter α has been introduced in the above calculation^{48,97}, which can be regarded as the vertex correction.

2. Charge-carrier diagonal and off-diagonal propagators

In the hole-doped case³⁹⁻⁴², it has been demonstrated that the interaction between the charge carriers directly

from the kinetic energy of the t - J model by the exchange

of a spin excitation induces the charge-carrier pairing state in the particle-particle channel. With the help of these discussions^{39–42}, the full charge-carrier diagonal and off-diagonal propagators of the t - J model (4) in the charge-carrier pairing state satisfy the self-consistent Dyson's equations, which can be derived in terms of the Eliashberg's approach⁴⁷ as,

$$g_a(\mathbf{k}, \omega) = g_a^{(0)}(\mathbf{k}, \omega) + g_a^{(0)}(\mathbf{k}, \omega) [\Sigma_{\text{ph}}^{(a)}(\mathbf{k}, \omega) g_a(\mathbf{k}, \omega) - \Sigma_{\text{pp}}^{(a)}(\mathbf{k}, \omega) \Gamma_a^\dagger(\mathbf{k}, \omega)], \quad (\text{A7a})$$

$$\Gamma_a^\dagger(\mathbf{k}, \omega) = g_a^{(0)}(\mathbf{k}, -\omega) [\Sigma_{\text{ph}}^{(a)}(\mathbf{k}, -\omega) \Gamma_a^\dagger(\mathbf{k}, \omega) + \Sigma_{\text{pp}}^{(a)}(\mathbf{k}, \omega) g_a(\mathbf{k}, \omega)], \quad (\text{A7b})$$

in the present electron-doped case, and then the full charge-carrier diagonal and off-diagonal propagators $g_a(\mathbf{k}, \omega)$ and $\Gamma_a^\dagger(\mathbf{k}, \omega)$ can be obtained directly as,

$$g_a(\mathbf{k}, \omega) = \frac{1}{\omega - \xi_{\mathbf{k}}^{(a)} - \Sigma_{\text{tot}}^{(a)}(\mathbf{k}, \omega)}, \quad (\text{A8a})$$

$$\Gamma_a^\dagger(\mathbf{k}, \omega) = \frac{L^{(a)}(\mathbf{k}, \omega)}{\omega - \xi_{\mathbf{k}}^{(a)} - \Sigma_{\text{tot}}^{(a)}(\mathbf{k}, \omega)}, \quad (\text{A8b})$$

respectively, where the charge-carrier total self-energy $\Sigma_{\text{tot}}^{(a)}(\mathbf{k}, \omega)$ and the function $L^{(a)}(\mathbf{k}, \omega)$ can be expressed as,

$$\Sigma_{\text{tot}}^{(a)}(\mathbf{k}, \omega) = \Sigma_{\text{ph}}^{(a)}(\mathbf{k}, \omega) + \frac{|\Sigma_{\text{pp}}^{(a)}(\mathbf{k}, \omega)|^2}{\omega + \xi_{\mathbf{k}}^{(a)} + \Sigma_{\text{ph}}^{(a)}(\mathbf{k}, -\omega)} \quad (\text{A9a})$$

$$L^{(a)}(\mathbf{k}, \omega) = -\frac{\Sigma_{\text{pp}}^{(a)}(\mathbf{k}, \omega)}{\omega + \xi_{\mathbf{k}}^{(a)} + \Sigma_{\text{ph}}^{(a)}(\mathbf{k}, -\omega)}, \quad (\text{A9b})$$

respectively, with the charge-carrier normal self-energy $\Sigma_{\text{ph}}^{(a)}(\mathbf{k}, \omega)$ in the particle-hole channel sketched in Fig. 11a and the charge-carrier anomalous self-energy $\Sigma_{\text{pp}}^{(a)}(\mathbf{k}, \omega)$ in the particle-particle channel sketched in Fig. 11b that have been derived in terms of the spin bubble as⁴⁸,

$$\Sigma_{\text{ph}}^{(a)}(\mathbf{k}, i\omega_n) = \frac{1}{N} \sum_{\mathbf{p}} \frac{1}{\beta} \sum_{ip_m} g_a(\mathbf{p} + \mathbf{k}, ip_m + i\omega_n) \times P^{(0)}(\mathbf{k}, \mathbf{p}, ip_m), \quad (\text{A10a})$$

$$\Sigma_{\text{pp}}^{(a)}(\mathbf{k}, i\omega_n) = \frac{1}{N} \sum_{\mathbf{p}} \frac{1}{\beta} \sum_{ip_m} \Gamma_a^\dagger(\mathbf{p} + \mathbf{k}, ip_m + i\omega_n) \times P^{(0)}(\mathbf{k}, \mathbf{p}, ip_m), \quad (\text{A10b})$$

respectively, where the effective spin propagator,

$$P^{(0)}(\mathbf{k}, \mathbf{p}, \omega) = \frac{1}{N} \sum_{\mathbf{q}} \Lambda_{\mathbf{p}+\mathbf{q}+\mathbf{k}}^2 \Pi(\mathbf{p}, \mathbf{q}, \omega), \quad (\text{A11})$$

as quoted in Eq. (8) of the main text, is closely related to the spin bubble $\Pi(\mathbf{p}, \mathbf{q}, \omega)$ in Eq. (11), and has been evaluated in subsection II B of the main text.

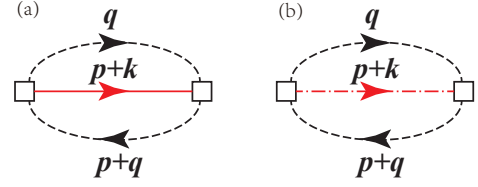


FIG. 11. The skeletal diagrams for the charge-carrier (a) normal and (b) anomalous self-energies for scattering charge carriers from the spin excitations. The red-solid-line and red-dash-dot-line represent the charge-carrier diagonal and off-diagonal propagators g_a and Γ_a^\dagger , respectively, and the black-dash-line depicts the spin propagator $D^{(0)}$, while \square describes the vertex function Λ .

The above results in Eqs. (A7) and (A10) indicate that the charge-carrier normal and anomalous self-energies $\Sigma_{\text{ph}}^{(a)}(\mathbf{k}, \omega)$ and $\Sigma_{\text{pp}}^{(a)}(\mathbf{k}, \omega)$ self-consistently link up with the full charge-carrier diagonal and off-diagonal propagators $g_a(\mathbf{k}, \omega)$ and $\Gamma_a^\dagger(\mathbf{k}, \omega)$. In particular, $\Sigma_{\text{ph}}^{(a)}(\mathbf{k}, \omega)$ is defined as the momentum and energy dependence of the charge-carrier pair gap, i.e., $\Sigma_{\text{pp}}^{(a)}(\mathbf{k}, \omega) = \bar{\Delta}_{\mathbf{k}}^{(a)}(\omega)$, while $\Sigma_{\text{ph}}^{(a)}(\mathbf{k}, \omega)$ depicts the momentum and energy dependence of the charge-carrier quasiparticle coherence, which therefore competes with charge-carrier pairing-state.

$\Sigma_{\text{pp}}^{(a)}(\mathbf{k}, \omega)$ is an even function of energy, however, $\Sigma_{\text{ph}}^{(a)}(\mathbf{k}, \omega)$ is not. In this case, $\Sigma_{\text{ph}}^{(a)}(\mathbf{k}, \omega)$ can be separated into its symmetric and antisymmetric parts as: $\Sigma_{\text{ph}}^{(a)}(\mathbf{k}, \omega) = \Sigma_{\text{phe}}^{(a)}(\mathbf{k}, \omega) + \omega \Sigma_{\text{pho}}^{(a)}(\mathbf{k}, \omega)$, and then both $\Sigma_{\text{phe}}^{(a)}(\mathbf{k}, \omega)$ and $\Sigma_{\text{pho}}^{(a)}(\mathbf{k}, \omega)$ are an even function of energy. In particular, this antisymmetric part $\Sigma_{\text{pho}}^{(a)}(\mathbf{k}, \omega)$ is associated closely with the momentum and energy dependence of the charge-carrier quasiparticle coherent weight as: $Z_{\text{F}}^{(a)-1}(\mathbf{k}, \omega) = 1 - \text{Re} \Sigma_{\text{pho}}^{(a)}(\mathbf{k}, \omega)$. In this paper, we focus mainly on the low-energy behaviors, and then $\bar{\Delta}_{\mathbf{k}}^{(a)}(\omega)$ and $Z_{\text{F}}^{(a)}(\mathbf{k}, \omega)$ can be generally discussed in the static limit as,

$$\bar{\Delta}_{\mathbf{k}}^{(a)} = \bar{\Delta}_{\mathbf{k}}^{(a)}(\omega = 0) = \bar{\Delta}_{\mathbf{a}} \gamma_{\mathbf{k}}^{(d)}, \quad (\text{A12a})$$

$$\frac{1}{Z_{\text{F}}^{(a)}(\mathbf{k})} = 1 - \text{Re} \Sigma_{\text{pho}}^{(a)}(\mathbf{k}, \omega = 0), \quad (\text{A12b})$$

respectively, with the charge-carrier pair gap parameter $\bar{\Delta}_{\mathbf{a}}$ and the d-wave factor $\gamma_{\mathbf{k}}^{(d)} = (\cos k_x - \cos k_y)/2$. Although $Z_{\text{F}}^{(a)}(\mathbf{k})$ still is a function of momentum, the momentum dependence is unimportant in a qualitative discussion. Following the ARPES experiments^{99,100}, the momentum \mathbf{k} in $Z_{\text{F}}^{(a)}(\mathbf{k})$ can be chosen as,

$$Z_{\text{F}}^{(a)} = Z_{\text{F}}^{(a)}(\mathbf{k}) |_{\mathbf{k}=[\pi, 0]}. \quad (\text{A13})$$

With the help of the above static-limit approximation, the renormalized charge-carrier diagonal and off-diagonal

propagators can be derived from Eq. (A8) as,

$$g_a^{(\text{RMF})}(\mathbf{k}, \omega) = Z_F^{(a)} \left(\frac{U_{\mathbf{a}\mathbf{k}}^2}{\omega - E_{\mathbf{k}}^{(a)}} + \frac{V_{\mathbf{a}\mathbf{k}}^2}{\omega + E_{\mathbf{k}}^{(a)}} \right), \quad (\text{A14a})$$

$$\Gamma_a^{(\text{RMF})\dagger}(\mathbf{k}, \omega) = -Z_F^{(a)} \frac{\bar{\Delta}_{Z\mathbf{k}}^{(a)}}{2E_{\mathbf{k}}^{(a)}} \left(\frac{1}{\omega - E_{\mathbf{k}}^{(a)}} - \frac{1}{\omega + E_{\mathbf{k}}^{(a)}} \right), \quad (\text{A14b})$$

where $E_{\mathbf{k}}^{(a)} = \sqrt{\bar{\xi}_{\mathbf{k}}^{(a)2} + |\bar{\Delta}_{Z\mathbf{k}}^{(a)}|^2}$ is the charge-carrier quasiparticle energy dispersion, $\bar{\xi}_{\mathbf{k}}^{(a)} = Z_F^{(a)} \xi_{\mathbf{k}}^{(a)}$ is the renormalized MF charge-carrier band energy, $\bar{\Delta}_{Z\mathbf{k}}^{(a)} = Z_F^{(a)} \bar{\Delta}_{\mathbf{k}}^{(a)}$ is the renormalized charge-carrier pair gap, and the charge-carrier quasiparticle coherence factors $U_{\mathbf{a}\mathbf{k}}$

and $V_{\mathbf{a}\mathbf{k}}$ are given by,

$$U_{\mathbf{a}\mathbf{k}}^2 = \frac{1}{2} \left(1 + \frac{\bar{\xi}_{\mathbf{k}}^{(a)}}{E_{\mathbf{k}}^{(a)}} \right), \quad (\text{A15a})$$

$$V_{\mathbf{a}\mathbf{k}}^2 = \frac{1}{2} \left(1 - \frac{\bar{\xi}_{\mathbf{k}}^{(a)}}{E_{\mathbf{k}}^{(a)}} \right), \quad (\text{A15b})$$

respectively. The above these charge-carrier quasiparticle coherence factors satisfy the constraint $U_{\mathbf{a}\mathbf{k}}^2 + V_{\mathbf{h}\mathbf{k}}^2 = 1$ for any momentum \mathbf{k} .

We now substitute the above charge-carrier renormalized diagonal and off-diagonal propagators in Eq. (A14) and spin propagator in Eq. (A4a) into Eq. (A10), and then obtain explicitly the charge-carrier normal self-energy $\Sigma_{\text{ph}}^{(a)}(\mathbf{k}, \omega)$ and the anomalous self-energy $\Sigma_{\text{pp}}^{(a)}(\mathbf{k}, \omega)$ as,

$$\begin{aligned} \Sigma_{\text{ph}}^{(a)}(\mathbf{k}, \omega) &= \frac{Z_F^{(a)}}{N^2} \sum_{\mathbf{p}\mathbf{p}'\nu} (-1)^{\nu+1} \Omega_{\mathbf{p}\mathbf{p}'\mathbf{k}} \left[U_{\mathbf{a}\mathbf{p}+\mathbf{k}}^2 \left(\frac{F_{1\nu}^{(a)}(\mathbf{p}, \mathbf{p}', \mathbf{k})}{\omega + \omega_{\mathbf{p}\mathbf{p}'}^{(\nu)} - E_{\mathbf{p}+\mathbf{k}}^{(a)}} - \frac{F_{2\nu}^{(a)}(\mathbf{p}, \mathbf{p}', \mathbf{k})}{\omega - \omega_{\mathbf{p}\mathbf{p}'}^{(\nu)} - E_{\mathbf{p}+\mathbf{k}}^{(a)}} \right) \right. \\ &\quad \left. + V_{\mathbf{a}\mathbf{p}+\mathbf{k}}^2 \left(\frac{F_{1\nu}^{(a)}(\mathbf{p}, \mathbf{p}', \mathbf{k})}{\omega - \omega_{\mathbf{p}\mathbf{p}'}^{(\nu)} + E_{\mathbf{p}+\mathbf{k}}^{(a)}} - \frac{F_{2\nu}^{(a)}(\mathbf{p}, \mathbf{p}', \mathbf{k})}{\omega + \omega_{\mathbf{p}\mathbf{p}'}^{(\nu)} + E_{\mathbf{p}+\mathbf{k}}^{(a)}} \right) \right], \end{aligned} \quad (\text{A16a})$$

$$\begin{aligned} \Sigma_{\text{pp}}^{(a)}(\mathbf{k}, \omega) &= \frac{Z_F^{(a)}}{N^2} \sum_{\mathbf{p}\mathbf{p}'\nu} (-1)^\nu \Omega_{\mathbf{p}\mathbf{p}'\mathbf{k}} \frac{\bar{\Delta}_{Z\mathbf{p}+\mathbf{k}}^{(a)}}{2E_{\mathbf{p}+\mathbf{k}}^{(a)}} \left[\left(\frac{F_{1\nu}^{(a)}(\mathbf{p}, \mathbf{p}', \mathbf{k})}{\omega + \omega_{\mathbf{p}\mathbf{p}'}^{(\nu)} - E_{\mathbf{p}+\mathbf{k}}^{(a)}} - \frac{F_{2\nu}^{(a)}(\mathbf{p}, \mathbf{p}', \mathbf{k})}{\omega - \omega_{\mathbf{p}\mathbf{p}'}^{(\nu)} - E_{\mathbf{p}+\mathbf{k}}^{(a)}} \right) \right. \\ &\quad \left. - \left(\frac{F_{1\nu}^{(a)}(\mathbf{p}, \mathbf{p}', \mathbf{k})}{\omega - \omega_{\mathbf{p}\mathbf{p}'}^{(\nu)} + E_{\mathbf{p}+\mathbf{k}}^{(a)}} - \frac{F_{2\nu}^{(a)}(\mathbf{p}, \mathbf{p}', \mathbf{k})}{\omega + \omega_{\mathbf{p}\mathbf{p}'}^{(\nu)} + E_{\mathbf{p}+\mathbf{k}}^{(a)}} \right) \right], \end{aligned} \quad (\text{A16b})$$

respectively, with $\nu = 1, 2$, $\Omega_{\mathbf{p}\mathbf{p}'\mathbf{k}} = \Lambda_{\mathbf{p}+\mathbf{p}'+\mathbf{k}}^2 B_{\mathbf{p}'} B_{\mathbf{p}+\mathbf{p}'} / (4\omega_{\mathbf{p}'} \omega_{\mathbf{p}+\mathbf{p}'})$, $\omega_{\mathbf{p}\mathbf{p}'}^{(\nu)} = \omega_{\mathbf{p}+\mathbf{p}'} - (-1)^\nu \omega_{\mathbf{p}'}$, and the functions,

$$F_{1\nu}^{(a)}(\mathbf{p}, \mathbf{p}', \mathbf{k}) = n_F[E_{\mathbf{p}+\mathbf{k}}^{(a)}] \{1 + n_B(\omega_{\mathbf{p}'+\mathbf{p}}) + n_B[(-1)^{\nu+1} \omega_{\mathbf{p}'}]\} + n_B(\omega_{\mathbf{p}'+\mathbf{p}}) n_B[(-1)^{\nu+1} \omega_{\mathbf{p}'}], \quad (\text{A17a})$$

$$F_{2\nu}^{(a)}(\mathbf{p}, \mathbf{p}', \mathbf{k}) = \{1 - n_F[E_{\mathbf{p}+\mathbf{k}}^{(a)}]\} \{1 + n_B(\omega_{\mathbf{p}'+\mathbf{p}}) + n_B[(-1)^{\nu+1} \omega_{\mathbf{p}'}]\} + n_B(\omega_{\mathbf{p}'+\mathbf{p}}) n_B[(-1)^{\nu+1} \omega_{\mathbf{p}'}]. \quad (\text{A17b})$$

3. Self-consistent equations for determination of charge-carrier pair gap parameter and the related order parameters

The above charge-carrier pair gap parameter $\bar{\Delta}_a$ and the charge-carrier quasiparticle coherent weight $Z_F^{(a)}$ satisfy following two self-consistent equations,

$$\bar{\Delta}_a = \frac{4Z_F^{(a)2}}{N^3} \sum_{\mathbf{p}\mathbf{p}'\mathbf{k}\nu} (-1)^\nu \Omega_{\mathbf{p}\mathbf{p}'\mathbf{k}} \frac{\gamma_{\mathbf{k}}^{(d)} \bar{\Delta}_a \gamma_{\mathbf{p}+\mathbf{k}}^{(d)}}{E_{\mathbf{p}+\mathbf{k}}^{(a)}} \left(\frac{F_{1\nu}^{(a)}(\mathbf{p}, \mathbf{p}', \mathbf{k})}{\omega_{\mathbf{p}\mathbf{p}'}^{(\nu)} - E_{\mathbf{p}+\mathbf{k}}^{(a)}} - \frac{F_{2\nu}^{(a)}(\mathbf{p}, \mathbf{p}', \mathbf{k})}{\omega_{\mathbf{p}\mathbf{p}'}^{(\nu)} + E_{\mathbf{p}+\mathbf{k}}^{(a)}} \right), \quad (\text{A18a})$$

$$\frac{1}{Z_F^{(a)}} = 1 + \frac{Z_F^{(a)}}{N^2} \sum_{\mathbf{p}\mathbf{p}'\nu} (-1)^{\nu+1} \Omega_{\mathbf{p}\mathbf{p}'\mathbf{k}_A} \left(\frac{F_{1\nu}^{(a)}(\mathbf{p}, \mathbf{p}', \mathbf{k}_A)}{[\omega_{\mathbf{p}\mathbf{p}'}^{(\nu)} - E_{\mathbf{p}+\mathbf{k}_A}^{(a)}]^2} + \frac{F_{2\nu}^{(a)}(\mathbf{p}, \mathbf{p}', \mathbf{k}_A)}{[\omega_{\mathbf{p}\mathbf{p}'}^{(\nu)} + E_{\mathbf{p}+\mathbf{k}_A}^{(a)}]^2} \right), \quad (\text{A18b})$$

respectively, where $\mathbf{k}_A = [\pi, 0]$. These two equations must be solved simultaneously with following self-consistent equations,

$$\phi_1 = \frac{Z_F^{(a)}}{2N} \sum_{\mathbf{k}} \gamma_{\mathbf{k}} \left(1 - \frac{\bar{\xi}_{\mathbf{k}}^{(a)}}{E_{\mathbf{k}}^{(a)}} \tanh \left[\frac{1}{2} \beta E_{\mathbf{k}}^{(a)} \right] \right), \quad (\text{A19a})$$

$$\phi_2 = \frac{Z_F^{(a)}}{2N} \sum_{\mathbf{k}} \gamma'_{\mathbf{k}} \left(1 - \frac{\bar{\xi}_{\mathbf{k}}^{(a)}}{E_{\mathbf{k}}^{(a)}} \tanh \left[\frac{1}{2} \beta E_{\mathbf{k}}^{(a)} \right] \right), \quad (\text{A19b})$$

$$\delta = \frac{Z_F^{(a)}}{2N} \sum_{\mathbf{k}} \left(1 - \frac{\bar{\xi}_{\mathbf{k}}^{(a)}}{E_{\mathbf{k}}^{(a)}} \tanh \left[\frac{1}{2} \beta E_{\mathbf{k}}^{(a)} \right] \right), \quad (\text{A19c})$$

$$\chi_1 = \frac{1}{N} \sum_{\mathbf{k}} \gamma_{\mathbf{k}} \frac{B_{\mathbf{k}}}{2\omega_{\mathbf{k}}} \coth \left[\frac{1}{2} \beta \omega_{\mathbf{k}} \right], \quad (\text{A19d})$$

$$\chi_2 = \frac{1}{N} \sum_{\mathbf{k}} \gamma'_{\mathbf{k}} \frac{B_{\mathbf{k}}}{2\omega_{\mathbf{k}}} \coth \left[\frac{1}{2} \beta \omega_{\mathbf{k}} \right], \quad (\text{A19e})$$

$$C_1 = \frac{1}{N} \sum_{\mathbf{k}} \gamma_{\mathbf{k}}^2 \frac{B_{\mathbf{k}}}{2\omega_{\mathbf{k}}} \coth \left[\frac{1}{2} \beta \omega_{\mathbf{k}} \right], \quad (\text{A19f})$$

$$C_2 = \frac{1}{N} \sum_{\mathbf{k}} \gamma_{\mathbf{k}}'^2 \frac{B_{\mathbf{k}}}{2\omega_{\mathbf{k}}} \coth \left[\frac{1}{2} \beta \omega_{\mathbf{k}} \right], \quad (\text{A19g})$$

$$C_3 = \frac{1}{N} \sum_{\mathbf{k}} \gamma_{\mathbf{k}} \gamma_{\mathbf{k}'} \frac{B_{\mathbf{k}}}{2\omega_{\mathbf{k}}} \coth \left[\frac{1}{2} \beta \omega_{\mathbf{k}} \right], \quad (\text{A19h})$$

$$\frac{1}{2} = \frac{1}{N} \sum_{\mathbf{k}} \frac{B_{\mathbf{k}}}{2\omega_{\mathbf{k}}} \coth \left[\frac{1}{2} \beta \omega_{\mathbf{k}} \right], \quad (\text{A19i})$$

$$\chi_1^z = \frac{1}{N} \sum_{\mathbf{k}} \gamma_{\mathbf{k}} \frac{B_{z\mathbf{k}}}{2\omega_{z\mathbf{k}}} \coth \left[\frac{1}{2} \beta \omega_{z\mathbf{k}} \right], \quad (\text{A19j})$$

$$\chi_2^z = \frac{1}{N} \sum_{\mathbf{k}} \gamma_{\mathbf{k}'} \frac{B_{z\mathbf{k}}}{2\omega_{z\mathbf{k}}} \coth \left[\frac{1}{2} \beta \omega_{z\mathbf{k}} \right], \quad (\text{A19k})$$

$$C_1^z = \frac{1}{N} \sum_{\mathbf{k}} \gamma_{\mathbf{k}}^2 \frac{B_{z\mathbf{k}}}{2\omega_{z\mathbf{k}}} \coth \left[\frac{1}{2} \beta \omega_{z\mathbf{k}} \right], \quad (\text{A19l})$$

$$C_3^z = \frac{1}{N} \sum_{\mathbf{k}} \gamma_{\mathbf{k}} \gamma_{\mathbf{k}'} \frac{B_{z\mathbf{k}}}{2\omega_{z\mathbf{k}}} \coth \left[\frac{1}{2} \beta \omega_{z\mathbf{k}} \right], \quad (\text{A19m})$$

then the charge-carrier pair gap parameter and the related order parameters, the decoupling parameter α , and the charge-carrier chemical potential μ_a are determined by the self-consistent calculation without using any adjustable parameters.

In the previous discussions^{30,46,57}, the above equations (A18) and (A19) have been evaluated self-consistently, and the obtained result of the evolution of the charge-carrier pair gap parameter $\bar{\Delta}_a$ in Eq. (A12a) with doping indicates that with the increase of doping, $\bar{\Delta}_a$ is raised gradually in the underdoped regime, and then reaches the maximum at around the optimal doping $\delta \approx 0.15$. However, with the further increase of doping, $\bar{\Delta}_a$ then turns into a monotonically decrease in the overdoped regime.

4. Charge-carrier pair transition temperature

The charge-carrier pair transition temperature $T_c^{(\text{pair})}$ as a function of doping³⁰ has been calculated self-

consistently from the above self-consistent equations (A18) and (A19) at the condition of the charge-carrier pair gap parameter $\bar{\Delta}_a = 0$, and the obtained result shows that $T_c^{(\text{pair})}$ as a function of doping presents a similar behavior of $\bar{\Delta}_a$, i.e., the maximal $T_c^{(\text{pair})}$ occurs around the optimal doping $\delta \approx 0.15$, and then decreases in both the underdoped and the overdoped regimes.

In the framework of the kinetic-energy driven superconductivity⁴⁰⁻⁴³, the spin excitation is directly coupled to charge-carrier pairs, where the interaction between the charge carriers in the particle-particle channel is attractive, then the system of charge carriers forms pairs of bound charge carriers. Since the coupling strength V_{eff} and charge-carrier pair order parameter Δ_a have been incorporated into the charge-carrier pair gap parameter $\bar{\Delta}_a$, the coupling strength V_{eff} can be evaluated in terms of the ratio of $\bar{\Delta}_a$ and Δ_a as^{40,42},

$$V_{\text{eff}} = \frac{\bar{\Delta}_a}{\Delta_a}, \quad (\text{A20})$$

where the charge-carrier pair order parameter Δ_a can be derived directly from the charge-carrier off-diagonal propagator (A14b) as,

$$\Delta_a = \frac{2}{N} \sum_{\mathbf{k}} [\gamma_{\mathbf{k}}^{(d)}]^2 \frac{[Z_F^{(a)}]^2 \bar{\Delta}_a}{E_{\mathbf{k}}^{(a)}} \tanh \left(\frac{1}{2} \beta E_{\mathbf{k}}^{(a)} \right). \quad (\text{A21})$$

The parent compounds of the electron-doped cuprate superconductors are a Mott insulator^{1,2} as we have mentioned in above Section I. When charge carriers are doped into this parent Mott insulator, there is a gain in the kinetic energy per charge carrier proportional to t due to hopping, however, at the same time, the magnetic energy is decreased, costing an energy of approximately J per site³⁸, therefore the doped charge carriers into a Mott insulator can be considered as a competition between the kinetic energy (δt) and magnetic energy (J). In this case, the essential physics of the dome-like shape doping dependence of $T_c^{(\text{pair})}$ can be attributed to the competition between the kinetic energy and magnetic energy^{40,42}. This follows a basic fact that the competition between the kinetic energy and magnetic energy also leads to that the spectral intensity of the spin excitation spectrum decreases with the increase of doping⁴⁸. However, as we^{40,42} have shown in the previous discussions that a decrease of the spin excitation spectral intensity with the increase of doping also leads to a decrease of the coupling strength V_{eff} with the increase of doping, i.e., the coupling strength V_{eff} smoothly decreases with the increase of doping from a strong-coupling case in the underdoped regime to a weak-coupling side in the overdoped regime⁸⁴⁻⁸⁶. On the other hand, the charge-carrier kinetic energy, which is proportional to doping δt , gradually increases with the increase of doping. In the underdoped regime, the coupling strength V_{eff} is very strong to bind the most charge carriers into charge-carrier pairs, and thus the number of charge-carrier pairs increases with the increase of doping, which leads to that

$T_c^{(\text{pair})}$ increases with the increase of doping^{40,42}. However, in the overdoped regime, the coupling strength V_{eff} is relatively weak. In this case, not all charge carriers can be bound to form charge-carrier pairs by this weakly attractive interaction, and then the number of charge-carrier pairs decreases with the increase of doping, which leads to that $T_c^{(\text{pair})}$ decreases with the further increase of doping^{40,42}. In particular, the optimal doping is a balance point, where the number of charge-carrier pairs and coupling strength V_{eff} are optimally matched^{40,42}. This is why $T_c^{(\text{pair})}$ takes a dome-like shape with the underdoped and overdoped regimes on each side of the optimal doping, where $T_c^{(\text{pair})}$ reaches its maximum³⁰.

Furthermore, it has been shown that this $T_c^{(\text{pair})}$ is the exactly same as that derived from the corresponding SC-state at the condition of the SC gap parameter $\bar{\Delta} = 0$, and will return to this discussion of $T_c^{(\text{pair})}$ towards subsection A 7 of this Appendix.

5. Derivation of full hole diagonal and off-diagonal propagators

In the previous studies for the hole-doped case⁴³ with the on-site local constraint $\sum_{\sigma} C_{l\sigma}^{\dagger} C_{l\sigma} \leq 1$, the full charge-spin recombination scheme has been established, where a charge carrier and a localized spin are fully recombined into a constrained electron. In this full charge-spin recombination scheme⁴³, we have realized that the coupling form between the electrons and spin excitations is the same as that between the charge carriers and spin excitations, which therefore indicates that the form of the self-consistent equations satisfied by the full electron diagonal and off-diagonal propagators is the same as the form satisfied by the full charge-carrier diagonal and off-diagonal propagators. In the present electron-doped case with the on-site local constraint $\sum_{\sigma} f_{l\sigma}^{\dagger} f_{l\sigma} \leq 1$ in the hole representation (2), we^{30,46,57} follow these previous discussions for the hole-doped case⁴³ and perform a full charge-spin recombination in which the full charge-carrier diagonal and off-diagonal propagators $g_a(\mathbf{k}, \omega)$ and $\Gamma_{\zeta}^{\dagger}(\mathbf{k}, \omega)$ in Eq. (A7) are replaced by the full hole diagonal and off-diagonal propagators $G_f(\mathbf{k}, \omega)$ and $\mathfrak{S}_f^{\dagger}(\mathbf{k}, \omega)$, respectively, and then the self-consistent Dyson's equations satisfied by the full hole diagonal and off-diagonal propagators of the t - J model (2) in the SC-state can be derived in terms of the Eliashberg's approach⁴⁷ as,

$$G_f(\mathbf{k}, \omega) = G_f^{(0)}(\mathbf{k}, \omega) + G_f^{(0)}(\mathbf{k}, \omega) [\Sigma_{\text{ph}}^{(f)}(\mathbf{k}, \omega) G_f(\mathbf{k}, \omega) - \Sigma_{\text{pp}}^{(f)}(\mathbf{k}, \omega) \mathfrak{S}_f^{\dagger}(\mathbf{k}, \omega)], \quad (\text{A22a})$$

$$\mathfrak{S}_f^{\dagger}(\mathbf{k}, \omega) = G_f^{(0)}(\mathbf{k}, -\omega) [\Sigma_{\text{ph}}^{(f)}(\mathbf{k}, -\omega) \mathfrak{S}_f^{\dagger}(\mathbf{k}, \omega) + \Sigma_{\text{pp}}^{(f)}(\mathbf{k}, \omega) G_f(\mathbf{k}, \omega)], \quad (\text{A22b})$$

where the hole non-interacting (diagonal) propagator of the t - J model $G_f^{(0)}(\mathbf{k}, \omega)$ can be expressed as

$G_f^{(0)-1}(\mathbf{k}, \omega) = \omega - \varepsilon_{\mathbf{k}}^{(f)}$. With the help of the above self-consistent equations (A22), we can obtain straightforwardly the full hole diagonal and off-diagonal propagators as,

$$G_f(\mathbf{k}, \omega) = \frac{1}{\omega - \varepsilon_{\mathbf{k}}^{(f)} - \Sigma_{\text{tot}}^{(f)}(\mathbf{k}, \omega)}, \quad (\text{A23a})$$

$$\mathfrak{S}_f^{\dagger}(\mathbf{k}, \omega) = \frac{L^{(f)}(\mathbf{k}, \omega)}{\omega - \varepsilon_{\mathbf{k}}^{(f)} - \Sigma_{\text{tot}}^{(f)}(\mathbf{k}, \omega)}, \quad (\text{A23b})$$

as quoted in Eq. (5) of the main text, where the total hole self-energy $\Sigma_{\text{tot}}^{(f)}(\mathbf{k}, \omega)$ and the function $L^{(f)}(\mathbf{k}, \omega)$ have been given in Eq. 6 of the main text. In particular, the hole normal self-energy $\Sigma_{\text{ph}}^{(f)}(\mathbf{k}, \omega)$ in the particle-hole channel sketched in Fig. 1a and hole anomalous self-energy $\Sigma_{\text{pp}}^{(f)}(\mathbf{k}, \omega)$ in the particle-particle channel sketched in Fig. 1b have been evaluated directly from the corresponding parts of the charge-carrier normal self-energy $\Sigma_{\text{ph}}^{(a)}(\mathbf{k}, \omega)$ and charge-carrier anomalous self-energy $\Sigma_{\text{pp}}^{(a)}(\mathbf{k}, \omega)$ in Eq. (A10) by the replacement of the full charge-carrier diagonal and off-diagonal propagators $g_a(\mathbf{k}, \omega)$ and $\Gamma_a^{\dagger}(\mathbf{k}, \omega)$ with the corresponding full hole diagonal and off-diagonal propagators $G_f(\mathbf{k}, \omega)$ and $\mathfrak{S}_f^{\dagger}(\mathbf{k}, \omega)$ as,

$$\Sigma_{\text{ph}}^{(f)}(\mathbf{k}, i\omega_n) = \frac{1}{N} \sum_{\mathbf{p}} \frac{1}{\beta} \sum_{ip_m} G_f(\mathbf{p} + \mathbf{k}, ip_m + i\omega_n) \times P^{(0)}(\mathbf{k}, \mathbf{p}, ip_m), \quad (\text{A24a})$$

$$\Sigma_{\text{pp}}^{(f)}(\mathbf{k}, i\omega_n) = \frac{1}{N} \sum_{\mathbf{p}} \frac{1}{\beta} \sum_{ip_m} \mathfrak{S}_f^{\dagger}(\mathbf{p} + \mathbf{k}, ip_m + i\omega_n) \times P^{(0)}(\mathbf{k}, \mathbf{p}, ip_m), \quad (\text{A24b})$$

respectively, as quoted in Eq. (7) of the main text.

In analogy to the derivation of the charge-carrier normal and anomalous self-energies in subsection A 2, the hole normal and anomalous self-energies have been also calculated explicitly in the previous studies^{30,46,57}. Following the discussions in subsection A 2, the hole normal self-energy $\Sigma_{\text{ph}}^{(f)}(\mathbf{k}, \omega)$ can be broken up into its symmetric and antisymmetric parts as: $\Sigma_{\text{ph}}^{(f)}(\mathbf{k}, \omega) = \Sigma_{\text{phe}}^{(f)}(\mathbf{k}, \omega) + \omega \Sigma_{\text{pho}}^{(f)}(\mathbf{k}, \omega)$, where all the symmetric part $\Sigma_{\text{phe}}^{(f)}(\mathbf{k}, \omega)$ and antisymmetric part $\Sigma_{\text{pho}}^{(f)}(\mathbf{k}, \omega)$ are an even function of energy. Moreover, the antisymmetric part $\Sigma_{\text{pho}}^{(f)}(\mathbf{k}, \omega)$ is identified as the hole quasiparticle coherent weight: $Z_{\text{F}}^{(f)-1}(\mathbf{k}, \omega) = 1 - \text{Re} \Sigma_{\text{pho}}^{(f)}(\mathbf{k}, \omega)$. In an interacting system, everything happens at around EFS. As a case for low-energy close to EFS, the hole pair gap and hole quasiparticle coherent weight can be discussed in the static-limit approximation,

$$\bar{\Delta}_{\mathbf{k}}^{(f)} = \Sigma_{\text{pp}}^{(f)}(\mathbf{k}, \omega = 0) = \bar{\Delta}_f \gamma_{\mathbf{k}}^{(d)}, \quad (\text{A25a})$$

$$\frac{1}{Z_{\text{F}}^{(f)}} = 1 - \text{Re} \Sigma_{\text{pho}}^{(f)}(\mathbf{k}, \omega = 0) |_{\mathbf{k}=[\pi, 0]}, \quad (\text{A25b})$$

where $\bar{\Delta}_f$ is the hole pair gap parameter, while the wave vector \mathbf{k} in $Z_F^{(f)}(\mathbf{k})$ has been chosen as $\mathbf{k} = [\pi, 0]$ just as it has been done in the ARPES experiments^{99,100}.

Based on the above static-limit approximation for the hole pair gap $\bar{\Delta}_k^{(f)}$ and hole quasiparticle coherent weight $Z_F^{(f)}$, we can obtain the renormalized hole diagonal and off-diagonal propagators from Eq. (A23) as,

$$G_f^{(\text{RMF})}(\mathbf{k}, \omega) = Z_F^{(f)} \left(\frac{U_{f\mathbf{k}}^2}{\omega - E_{\mathbf{k}}^{(f)}} + \frac{V_{f\mathbf{k}}^2}{\omega + E_{\mathbf{k}}^{(f)}} \right), \quad (\text{A26a})$$

$$\mathfrak{S}_f^{(\text{RMF})\dagger}(\mathbf{k}, \omega) = -Z_F^{(f)} \frac{\bar{\Delta}_Z^{(f)}(\mathbf{k})}{2E_{\mathbf{k}}^{(f)}} \left(\frac{1}{\omega - E_{\mathbf{k}}^{(f)}} - \frac{1}{\omega + E_{\mathbf{k}}^{(f)}} \right), \quad (\text{A26b})$$

with the renormalized hole band energy $\bar{\varepsilon}_{\mathbf{k}}^{(f)} =$

$Z_F^{(f)} \bar{\varepsilon}_{\mathbf{k}}^{(f)}$, the renormalized hole pair gap $\bar{\Delta}_Z^{(f)}(\mathbf{k}) = Z_F^{(f)} \bar{\Delta}_{\mathbf{k}}^{(f)}$, the hole quasiparticle energy spectrum $E_{\mathbf{k}}^{(f)} = \sqrt{\bar{\varepsilon}_{\mathbf{k}}^{(f)2} + |\bar{\Delta}_Z^{(f)}(\mathbf{k})|^2}$, and the hole quasiparticle coherence factors

$$U_{f\mathbf{k}}^2 = \frac{1}{2} \left(1 + \frac{\bar{\varepsilon}_{\mathbf{k}}^{(f)}}{E_{\mathbf{k}}^{(f)}} \right), \quad (\text{A27a})$$

$$V_{f\mathbf{k}}^2 = \frac{1}{2} \left(1 - \frac{\bar{\varepsilon}_{\mathbf{k}}^{(f)}}{E_{\mathbf{k}}^{(f)}} \right), \quad (\text{A27b})$$

with the constraint $U_{f\mathbf{k}}^2 + V_{f\mathbf{k}}^2 = 1$ for any wave vector \mathbf{k} .

We now substitute the above renormalized hole diagonal and off-diagonal propagators in Eq. (A26) and spin propagator in Eq. (A4a) into Eqs. (A24), and then obtain the hole normal and anomalous self-energies as,

$$\begin{aligned} \Sigma_{\text{ph}}^{(f)}(\mathbf{k}, \omega) &= \frac{Z_F^{(f)}}{N^2} \sum_{\mathbf{p}\mathbf{p}'\nu} (-1)^{\nu+1} \Omega_{\mathbf{p}\mathbf{p}'\mathbf{k}} \left[U_{f\mathbf{p}+\mathbf{k}}^2 \left(\frac{F_{1\nu}^{(f)}(\mathbf{p}, \mathbf{p}', \mathbf{k})}{\omega + \omega_{\mathbf{p}\mathbf{p}'}^{(\nu)} - E_{\mathbf{p}+\mathbf{k}}^{(f)}} - \frac{F_{2\nu}^{(f)}(\mathbf{p}, \mathbf{p}', \mathbf{k})}{\omega - \omega_{\mathbf{p}\mathbf{p}'}^{(\nu)} - E_{\mathbf{p}+\mathbf{k}}^{(f)}} \right) \right. \\ &\quad \left. + V_{f\mathbf{p}+\mathbf{k}}^2 \left(\frac{F_{1\nu}^{(f)}(\mathbf{p}, \mathbf{p}', \mathbf{k})}{\omega - \omega_{\mathbf{p}\mathbf{p}'}^{(\nu)} + E_{\mathbf{p}+\mathbf{k}}^{(f)}} - \frac{F_{2\nu}^{(f)}(\mathbf{p}, \mathbf{p}', \mathbf{k})}{\omega + \omega_{\mathbf{p}\mathbf{p}'}^{(\nu)} + E_{\mathbf{p}+\mathbf{k}}^{(f)}} \right) \right], \end{aligned} \quad (\text{A28a})$$

$$\begin{aligned} \Sigma_{\text{pp}}^{(f)}(\mathbf{k}, \omega) &= \frac{Z_F^{(f)}}{N^2} \sum_{\mathbf{p}\mathbf{p}'\nu} (-1)^\nu \Omega_{\mathbf{p}\mathbf{p}'\mathbf{k}} \frac{\bar{\Delta}_Z^{(f)}(\mathbf{p} + \mathbf{k})}{2E_{\mathbf{p}+\mathbf{k}}^{(f)}} \left[\left(\frac{F_{1\nu}^{(f)}(\mathbf{p}, \mathbf{p}', \mathbf{k})}{\omega + \omega_{\mathbf{p}\mathbf{p}'}^{(\nu)} - E_{\mathbf{p}+\mathbf{k}}^{(f)}} - \frac{F_{2\nu}^{(f)}(\mathbf{p}, \mathbf{p}', \mathbf{k})}{\omega - \omega_{\mathbf{p}\mathbf{p}'}^{(\nu)} - E_{\mathbf{p}+\mathbf{k}}^{(f)}} \right) \right. \\ &\quad \left. - \left(\frac{F_{1\nu}^{(f)}(\mathbf{p}, \mathbf{p}', \mathbf{k})}{\omega - \omega_{\mathbf{p}\mathbf{p}'}^{(\nu)} + E_{\mathbf{p}+\mathbf{k}}^{(f)}} - \frac{F_{2\nu}^{(f)}(\mathbf{p}, \mathbf{p}', \mathbf{k})}{\omega + \omega_{\mathbf{p}\mathbf{p}'}^{(\nu)} + E_{\mathbf{p}+\mathbf{k}}^{(f)}} \right) \right], \end{aligned} \quad (\text{A28b})$$

respectively, with $\nu = 1, 2$, and the functions,

$$F_{1\nu}^{(f)}(\mathbf{p}, \mathbf{p}', \mathbf{k}) = n_F(E_{\mathbf{p}+\mathbf{k}}^{(f)}) \{1 + n_B(\omega_{\mathbf{p}'+\mathbf{p}}) + n_B[(-1)^{\nu+1} \omega_{\mathbf{p}'}]\} + n_B(\omega_{\mathbf{p}'+\mathbf{p}}) n_B[(-1)^{\nu+1} \omega_{\mathbf{p}'}], \quad (\text{A29a})$$

$$F_{2\nu}^{(f)}(\mathbf{p}, \mathbf{p}', \mathbf{k}) = [1 - n_F(E_{\mathbf{p}+\mathbf{k}}^{(f)})] \{1 + n_B(\omega_{\mathbf{p}'+\mathbf{p}}) + n_B[(-1)^{\nu+1} \omega_{\mathbf{p}'}]\} + n_B(\omega_{\mathbf{p}'+\mathbf{p}}) n_B[(-1)^{\nu+1} \omega_{\mathbf{p}'}]. \quad (\text{A29b})$$

6. Self-consistent equations for determination of hole order parameters

The above hole quasiparticle coherent weight, the hole pair gap parameter, and the hole chemical potential fulfills following three self-consistent equations,

$$\frac{1}{Z_F^{(f)}} = 1 + \frac{Z_F^{(f)}}{N^2} \sum_{\mathbf{p}\mathbf{p}'\nu} (-1)^{\nu+1} \Omega_{\mathbf{p}\mathbf{p}'\mathbf{k}_A} \left(\frac{F_{1\nu}^{(f)}(\mathbf{p}, \mathbf{p}', \mathbf{k}_A)}{(\omega_{\mathbf{p}\mathbf{p}'}^{(\nu)} - E_{\mathbf{p}+\mathbf{k}_A}^{(f)})^2} + \frac{F_{2\nu}^{(f)}(\mathbf{p}, \mathbf{p}', \mathbf{k}_A)}{(\omega_{\mathbf{p}\mathbf{p}'}^{(\nu)} + E_{\mathbf{p}+\mathbf{k}_A}^{(f)})^2} \right), \quad (\text{A30a})$$

$$\bar{\Delta}_f = \frac{4Z_F^{(f)2}}{N^3} \sum_{\mathbf{p}\mathbf{p}'\mathbf{k}\nu} (-1)^\nu \Omega_{\mathbf{p}\mathbf{p}'\mathbf{k}} \frac{\gamma_{\mathbf{k}}^{(d)} \bar{\Delta}_f \gamma_{\mathbf{p}+\mathbf{k}}^{(d)}}{E_{\mathbf{p}+\mathbf{k}}^{(f)}} \left(\frac{F_{1\nu}^{(f)}(\mathbf{p}, \mathbf{p}', \mathbf{k})}{\omega_{\mathbf{p}\mathbf{p}'}^{(\nu)} - E_{\mathbf{p}+\mathbf{k}}^{(f)}} - \frac{F_{2\nu}^{(f)}(\mathbf{p}, \mathbf{p}', \mathbf{k})}{\omega_{\mathbf{p}\mathbf{p}'}^{(\nu)} + E_{\mathbf{p}+\mathbf{k}}^{(f)}} \right), \quad (\text{A30b})$$

$$1 - \delta = \frac{Z_F^{(f)}}{N} \sum_{\mathbf{k}} \left(1 - \frac{\bar{\varepsilon}_{\mathbf{k}}^{(f)}}{E_{\mathbf{k}}^{(f)}} \tanh \left[\frac{1}{2} \beta E_{\mathbf{k}}^{(f)} \right] \right), \quad (\text{A30c})$$

where $\mathbf{k}_A = [\pi, 0]$. With the same calculation condition as in the evaluation of the self-consistent equations (A18)

and (A19), the above equations (A30) have been also calculated self-consistently^{30,46,57}, where the hole quasi-particle coherent weight, the hole pair gap parameter, and hole chemical potential are obtained without using any adjustable parameters. In particular, the dome-like shape doping dependence of the charge-carrier pair gap parameter $\bar{\Delta}_a$ thus also induces the same dome-like shape doping dependence of the hole pair gap parameter $\bar{\Delta}_f$.

7. Superconducting transition temperature

As we^{30,46,57} have shown in Eq. (15b) of the main text, the electron anomalous self-energy is obtained from the hole anomalous self-energy in terms of the particle-hole transformation as: $\Sigma_{pp}(\mathbf{k}, \omega) = \Sigma_{pp}^{(f)}(\mathbf{k}, \omega)$, which indicates that the electron pair gap $\bar{\Delta}_k$ is identical with the hole pair gap $\bar{\Delta}_k^{(f)}$, i.e., $\bar{\Delta}_k = \bar{\Delta}_k^{(f)}$. In this case, the SC transition temperature T_c as a function of doping can be derived self-consistently from the above self-consistent equations in Eq. (A30) at the condition of the hole pair gap $\bar{\Delta}_k^{(f)} = 0$ [then the electron pair gap

$\bar{\Delta}_k = 0$]. In the recent discussions³⁰, we have found that in a given doping concentration, the magnitude of the SC transition temperature T_c in Fig. 3 evaluated from the above self-consistent equations in Eq. (A30) is exactly identical with the magnitude of the charge-carrier pair transition temperature $T_c^{(\text{pair})}$ calculated from the corresponding self-consistent equations in Eqs. (A18) and (A19) at the condition of the charge-carrier pair gap $\bar{\Delta}_k^{(a)} = 0$. This follows a basic fact that in the framework of the kinetic-energy-driven superconductivity^{40–43}, the effective attractive interaction between charge carriers originates in their coupling to the spin excitation. On the other hand, the hole (then the electron) pairing interaction in the full charge-spin recombination scheme⁴³ is mediated by the exchange of the same spin excitation, which thus induces that the SC transition temperature T_c shown in Fig. 3 is the same as the charge-carrier pair transition temperature $T_c^{(\text{pair})}$, and then the dome-like shape of the doping dependence of T_c with its maximum occurring at around the optimal doping is a natural consequence of the dome-like shape of the doping dependence of $T_c^{(\text{pair})}$ with its maximum occurring at around the same optimal doping.

* Corresponding author. Email: spfeng@bnu.edu.cn

¹ See, e.g., the review, M. Fujita, H. Hiraka, M. Matsuda, M. Matsuura, J. M. Tranquada, S. Wakimoto, G. Xu, and K. Yamada, *Progress in Neutron Scattering Studies of Spin Excitations in High- T_c Cuprates*, J. Phys. Soc. Jpn. 81 (2012), pp. 011007.

² P. W. Anderson, *The Resonating Valence Bond State in La_2CuO_4 and Superconductivity*, Science 235 (1987), pp. 1196-1198.

³ J. G. Bednorz and K. A. Müller, *Possible High T_c Superconductivity in the Ba-La-Cu-O System*, Z. Phys. B 64 (1986), pp. 189-193.

⁴ Y. Tokura, H. Takagi, and S. Uchida, *A superconducting copper oxide compound with electrons as the charge carriers*, Nature 337 (1989), pp. 345-347.

⁵ N. P. Armitage, P. Fournier, and R. L. Greene, *Progress and perspectives on electron-doped cuprates*, Rev. Mod. Phys. 82 (2010), pp. 2421-2487.

⁶ T. Adachi, Y. Mori, A. Takahashi, M. Kato, T. Nishizaki, T. Sasaki, N. Kobayashi, and Y. Koike, *Evolution of the Electronic State through the Reduction Annealing in Electron-Doped $\text{Pr}_{1.3-x}\text{La}_{0.7}\text{Ce}_x\text{CuO}_{4+\delta}$ ($x=0.10$) Single Crystals: Antiferromagnetism, Kondo Effect, and Superconductivity*, J. Phys. Soc. Jpn. 82 (2013), pp. 063713.

⁷ T. Adachi, T. Kawamata, Y. Koike, *Novel Electronic State and Superconductivity in the Electron-Doped High- T_c T^* -Superconductors*, Condensed Matter 2 (2017), pp. 23.

⁸ M. Horio, T. Adachi, Y. Mori, A. Takahashi, T. Yoshida, H. Suzuki, L. C. C. Ambolode II, K. Okazaki, K. Ono, H. Kumigashira, H. Anzai, M. Arita, H. Namatame, M. Taniguchi, D. Ootsuki, K. Sawada, M. Takahashi, T. Mizokawa, Y. Koike and A. Fujimori, *Suppression of the antiferromagnetic pseudogap in the electron-doped high-*

temperature superconductor by protect annealing, Nat. Commun. 7 (2016), pp. 10567.

⁹ D. Song, G. Han, W. Kyung, J. Seo, S. Cho, B. S. Kim, M. Arita, K. Shimada, H. Namatame, M. Taniguchi, Y. Yoshida, H. Eisaki, S. R. Park, and C. Kim, *Electron number-based phase diagram of $\text{Pr}_{1-x}\text{LaCe}_x\text{CuO}_{4-\delta}$ and possible absence of disparity between electron-and hole-doped cuprate phase diagrams*, Phys. Rev. Lett. 118 (2017), pp. 137001.

¹⁰ C. Lin, T. Adachi, M. Horio, T. Ohgi, M.A. Baqiya, T. Kawamata, H. Sato, T. Sumura, K. Koshiishi, S. Nakata, G. Shibata, K. Hagiwara, M. Suzuki, K. Ono, K. Horiba, H. Kumigashira, S. Ideta, K. Tanaka, Y. Koike, A. Fujimori, *Extended superconducting dome revealed by angle-resolved photoemission spectroscopy of electron-doped cuprates prepared by the protect annealing method*, Phys. Rev. Research 3 2021, pp. 013180.

¹¹ M. Horio, K. P. Kramer, Q. Wang, A. Zaidan, K. von Arx, D. Sutter, C. E. Matt, Y. Sassa, N. C. Plumb, M. Shi, A. Hanff, S. K. Mahatha, H. Bentmann, F. Reinert, S. Rohlf, F. K. Diekmann, J. Buck, M. Kalläne, K. Rossnagel, E. Rienks, V. Granata, R. Fittipaldi, A. Vecchione, T. Ohgi, T. Kawamata, T. Adachi, Y. Koike, A. Fujimori, M. Hoesch, J. Chang, *Oxide Fermi liquid universality revealed by electron spectroscopy*, Phys. Rev. B 102 (2020), pp. 245153.

¹² I. K. Drozdov, I. Pletikosić, C. -K. Kim, K. Fujita, G. D. Gu, J. C. S. Davis, P. D. Johnson, I. Božović, and T. Valla, *Phase diagram of $\text{Bi}_2\text{Sr}_2\text{CaCu}_2\text{O}_{8+\delta}$ revisited*, Nat. Commun. 9 (2018), pp. 5210.

¹³ L. Taillefer, *Scattering and pairing in cuprate superconductors*, Annu. Rev. Condens. Matter Phys. 1 (2010), pp. 51-70.

- ¹⁴ P. Li, F. F. Balakirev, and R. L. Greene, *High-field Hall resistivity and magnetoresistance of electron-doped $Pr_{2-x}Ce_xCuO_{4-\delta}$* , Phys. Rev. Lett. 99 (2007), pp. 047003.
- ¹⁵ N. R. Poniatowski, T. Sarkar, and R. L. Greene, *Anomalous normal-state magnetotransport in an electron-doped cuprate*, Phys. Rev. B 103 (2021), pp. 125102.
- ¹⁶ N. R. Poniatowski, T. Sarkar, S. Das Sarma, and R. L. Greene, *Resistivity saturation in an electron-doped cuprate*, Phys. Rev. B 103 (2021), pp. L020501.
- ¹⁷ R. L. Greene, P. R. Mandal, N. R. Poniatowski, and T. Sarkar, *The strange metal state of the electron-doped cuprates*, Annu. Rev. Condens. Matter Phys. 11 (2020), pp. 213-229.
- ¹⁸ P. Fournier, P. Mohanty, E. Maiser, S. Darzens, T. Venkatesan, C. J. Lobb, G. Czjzek, R. A. Webb, and R. L. Greene, *Insulator-Metal crossover near optimal doping in $Pr_{2-x}Ce_xCuO_4$: Anomalous normal-state low temperature resistivity*, Phys. Rev. Lett. 81 (1998), pp. 4720.
- ¹⁹ K. Jin, N. P. Butch, K. Kirshenbaum, J. Paglione, and R. L. Greene, *Link between spin fluctuations and electron pairing in copper oxide superconductors*, Nature 476 (2011), pp. 73-75.
- ²⁰ T. Sarkar, P. R. Mandal, J. S. Higgins, Y. Zhao, H. Yu, K. Jin, and R. L. Greene, *Fermi surface reconstruction and anomalous low-temperature resistivity in electron-doped $La_{2-x}Ce_xCuO_4$* , Phys. Rev. B 96 (2017), pp. 155449.
- ²¹ T. Sarkar, P. R. Mandal, N. R. Poniatowski, M. K. Chan, R. L. Greene, *Correlation between scale-invariant normal-state resistivity and superconductivity in an electron-doped cuprate*, Sci. Adv. 5 (2019), pp. eaav6753.
- ²² A. Legros, S. Benhabib, W. Tabis, F. Laliberté, M. Dion, M. Lizaïre, B. Vignolle, D. Vignolles, H. Raffy, Z. Z. Li, P. Auban-Senzier, N. Doiron-Leyraud, P. Fournier, D. Colson, L. Taillefer, and C. Proust, *Universal T-linear resistivity and Planckian dissipation in overdoped cuprates*, Nat. Phys. 15 (2019), pp. 142-147.
- ²³ J. Yuan, Q. Chen, K. Jiang, Z. Feng, Z. Lin, H. Yu, G. He, J. Zhang, X. Jiang, X. Zhang, Y. Shi, Y. Zhang, M. Qin, Z. Cheng, N. Tamura, Y.-F. Yang, T. Xiang, J. Hu, I. Takeuchi, K. Jin, and Z. Zhao, *Scaling of the strange-metal scattering in unconventional superconductors*, Nature 602 (2022), pp. 431-436.
- ²⁴ J. R. Schrieffer, *Theory of Superconductivity*, Benjamin, New York, 1964.
- ²⁵ A. A. Abrikosov, *Fundamentals of the Theory of Metals*, Elsevier Science Publishers B. V., 1988.
- ²⁶ G. D. Mahan, *Many-Particle Physics*, Plenum Press, New York, 1981.
- ²⁷ B. Keimer, S. A. Kivelson, M. R. Norman, S. Uchida, and J. Zaanen, *From quantum matter to high-temperature superconductivity in copper oxides*, Nature 518 (2015), pp. 179-186.
- ²⁸ C. M. Varma, *Colloquium: Linear in temperature resistivity and associated mysteries including high temperature superconductivity*, Rev. Mod. Phys. 92 (2020), pp. 031001.
- ²⁹ P. W. Phillips, N. E. Hussey, and P. Abbamonte, *Stranger than metals*, Science 377 (2022), pp. eabh4273.
- ³⁰ S. Tan, Y. Liu, Y. Mou, and S. Feng, *Anisotropic dressing of electrons in electron-doped cuprate superconductors*, Phys. Rev. B 103 (2021), pp. 014503.
- ³¹ X. Ma, M. Zeng, Z. Cao, and S. Feng, *Low-temperature T-linear resistivity in the strange metal phase of overdoped cuprate superconductors due to umklapp scattering from a spin excitation*, Phys. Rev. B 108 (2023), pp. 134502.
- ³² M. S. Hybertsen, E. B. Stechel, M. Schluter, and D. R. Jennison, *Renormalization from density-functional theory to strong-coupling models for electronic states in Cu-O materials*, Phys. Rev. B 41 (1990), pp. 11068.
- ³³ R. J. Gooding, K. J. E. Vos, and P. W. Leung, *Theory of electron-hole asymmetry in doped CuO_2 planes*, Phys. Rev. B 50 (1994), pp. 12866.
- ³⁴ C. Kim, P. J. White, Z.-X. Shen, T. Tohyama, Y. Shibata, S. Maekawa, B. O. Wells, Y. J. Kim, R. J. Birgeneau, and M. A. Kastner, *Systematics of the photoemission spectral function of cuprates: Insulators and hole- and electron-doped superconductors*, Phys. Rev. Lett. 80 (1998), pp. 4245-4248.
- ³⁵ L. Yu, *Many-body problems in high temperature superconductors*, in *Recent Progress in Many-Body Theories*, edited by T. L. Ainsworth, C. E. Campbell, B. E. Clements, and E. Krotscheck, Plenum, New York, 1992, Vol. 3, p. 157.
- ³⁶ S. Feng, J.B. Wu, Z.B. Su, and L. Yu, *Slave-particle studies of the electron-momentum distribution in the low-dimensional t-J model*, Phys. Rev. B 47 (1993), pp. 15192-15200.
- ³⁷ L. Zhang, J. K. Jain, and V. J. Emery, *Importance of the local constraint in slave-boson theories*, Phys. Rev. B 47 (1993), pp. 3368-3373.
- ³⁸ P. A. Lee, N. Nagaosa, and X.-G. Wen, *Doping a Mott insulator: Physics of high-temperature superconductivity*, Rev. Mod. Phys. 78 (2006), pp. 17-85.
- ³⁹ S. Feng, J. Qin, and T. Ma, *A gauge invariant dressed holon and spinon description of the normal state of underdoped cuprates*, J. Phys.: Condens. Matter 16 (2004), pp. 343; S. Feng, Z. B. Su, and L. Yu, *Fermion-spin transformation to implement the charge-spin separation*, Phys. Rev. B 49 (1994), pp. 2368-2384.
- ⁴⁰ S. Feng, Y. Lan, H. Zhao, L. Kuang, L. Qin, and X. Ma, *Kinetic-energy-driven superconductivity in cuprate superconductors*, Int. J. Mod. Phys. B 29 (2015), pp. 1530009.
- ⁴¹ S. Feng, *Kinetic energy driven superconductivity in doped cuprates*, Phys. Rev. B 68 (2003), pp. 184501; S. Feng, T. Ma, and H. Guo, *Magnetic nature of superconductivity in doped cuprates*, Physica C 436 (2006), pp. 14-24.
- ⁴² S. Feng, H. Zhao, and Z. Huang, *Two gaps with one energy scale in cuprate superconductors*, Phys. Rev. B 85 (2012), pp. 054509; Phys. Rev. B 85, (2012), pp. 099902(E).
- ⁴³ S. Feng, L. Kuang, and H. Zhao, *Electronic structure of cuprate superconductors in a full charge-spin recombination scheme*, Physica C 517 (2015), pp. 5-17.
- ⁴⁴ J. R. Schrieffer, *Wards identity and the suppression of spin fluctuation superconductivity*, J. Low Temp. Phys. 99 (1995), PP.397-402.
- ⁴⁵ K.-J. Xu, Q. Guo, M. Hashimoto, Z.-X. Li, S.-D. Chen, J. He, Y. He, C. Li, M. H. Berntsen, C. R. Rotundu, Y. S. Lee, T. P. Devereaux, A. Rydh, D.-H. Lu, D.-H. Lee, O. Tjernberg, Z.-X. Shen, *Bogoliubov quasiparticle on the gossamer Fermi surface in electron-doped cuprates*, Nature Phys. 19 (2023), PP. 1834-1840.
- ⁴⁶ S. Tan, Y. Mou, Y. Liu, and S. Feng, *ARPES autocorrelation in electron-doped cuprate superconductors*, J. Supercond. Nov. Magn. 33 (2020), PP. 2305-2311.
- ⁴⁷ G. M. Eliashberg, *Interactions between electrons and lattice vibrations in a superconductor*, Sov. Phys. JETP 11 (1960), pp. 696-702.
- ⁴⁸ L. Cheng and S. Feng, *Doping and energy evolution of spin dynamics in the electron-doped cuprate superconductors*

- tor $Pr_{0.88}LaCe_{0.12}CuO_{4-\delta}$, Phys. Rev. B 77 (2008), pp. 054518.
- ⁴⁹ J. Brinckmann and P. A. Lee, *Renormalized mean-field theory of neutron scattering in cuprate superconductors*, Phys. Rev. B 65 (2001), pp. 014502.
- ⁵⁰ F. Restrepo, J. Zhao, J. C. Campuzano, and U. Chatterjee, *Temperature and carrier concentration dependence of Fermi arcs in moderately underdoped $Bi_2Sr_2CaCu_2O_{8+\delta}$ cuprate high-temperature superconductors: A joint density of states perspective*, Phys. Rev. B 107 (2023), pp. 174519.
- ⁵¹ J. C. Campuzano, M. R. Norman, M. Randeira, *Photoemission in the High- T_c Superconductors*, in *Physics of Superconductors*, vol. II, edited by K. H. Bennemann and J. B. Ketterson, Springer, Berlin Heidelberg New York, 2004, pp. 167–273.
- ⁵² A. Damascelli, Z. Hussain, and Z.-X. Shen, *Angle-resolved photoemission studies of the cuprate superconductors*, Rev. Mod. Phys. 75 (2003), pp. 473–541.
- ⁵³ J. Fink, S. Borisenko, A. Kordyuk, A. Koitzsch, J. Geck, V. Zabalotnyy, M. Knupfer, B. Buechner, and H. Berger, *Dressing of the Charge Carriers in High- T_c Superconductors*, in *Lecture Notes in Physics*, vol. 715, edited by S. Hüfner, Springer-Verlag Berlin Heidelberg, 2007, pp. 295–325.
- ⁵⁴ N. E. Hussey, *Phenomenology of the normal state in-plane transport properties of high- T_c cuprates*, J. Phys.: Condens. Matter 20 (2008), pp. 123201.
- ⁵⁵ T. Timusk and B. Statt, *The pseudogap in high-temperature superconductors: an experimental survey*, Rep. Prog. Phys. 62 (1999), pp. 61–122.
- ⁵⁶ M. A. Kastner, R. J. Birgeneau, G. Shirane, and Y. Endoh, *Magnetic, Magnetic, transport, and optical properties of monolayer copper oxides*, Rev. Mod. Phys. 70 (1998), pp. 897–928.
- ⁵⁷ Y. Mou and S. Feng, *Doping dependence of charge order in electron-doped cuprate superconductors*, Phil. Mag. 97 (2017), pp. 3361–3380.
- ⁵⁸ R. Mahajan, M. Barkeshli, and S. A. Hartnoll, *Non-Fermi liquids and the Wiedemann-Franz law*, Phys. Rev. B 88 (2013), pp. 125107.
- ⁵⁹ S. A. Hartnoll, R. Mahajan, M. Punk, and S. Sachdev, *Transport near the Ising-nematic quantum critical point of metals in two dimensions*, Phys. Rev. B 89 (2014), pp. 155130.
- ⁶⁰ A. A. Patel and S. Sachdev, *DC resistivity at the onset of spin density wave order in two-dimensional metals*, Phys. Rev. B 90 (2014), pp. 165146.
- ⁶¹ A. Lucas and S. Sachdev, *Memory matrix theory of magnetotransport in strange metals*, Phys. Rev. B 91 (2015), pp. 195122.
- ⁶² L. E. Vieira, V. S. de Carvalho, H. Freire, *DC resistivity near a nematic quantum critical point: Effects of weak disorder and acoustic phonons*, Ann. Phys. 419 (2020), pp. 168230.
- ⁶³ I. Mandal and H. Freire, *Transport in the non-Fermi liquid phase of isotropic Luttinger semimetals*, Phys. Rev. B 103 (2021), pp. 195116.
- ⁶⁴ R. E. Prange and L. P. Kadanoff, *Transport theory for electron-phonon interactions in metals*, Phys. Rev. 134 (1964), pp. A566–A580.
- ⁶⁵ P. A. Lee, *Low-temperature T -linear resistivity due to umklapp scattering from a critical mode*, Phys. Rev. B 104 (2021), pp. 035140.
- ⁶⁶ T. M. Rice, N. J. Robinson, and A. M. Tsvelik, *Umklapp scattering as the origin of T -linear resistivity in the normal state of high- T_c cuprate superconductors*, Phys. Rev. B 96 (2017), pp. 220502(R).
- ⁶⁷ N. E. Hussey, *The normal state scattering rate in high-cuprates*, Eur. Phys. J. B 31 (2003), pp. 495–507.
- ⁶⁸ F. D. M. Haldane, *Fermi-surface geometry and “Planckian dissipation”*, arXiv:1811.12120.
- ⁶⁹ R. Daou, N. Doiron-Leyraud, D. LeBoeuf, S. Y. Li, F. Laliberté, O. Cyr-Choinière, Y. J. Jo, L. Balicas, J.-Q. Yan, J.-S. Zhou, J. B. Goodenough, and L. Taillefer, *Linear temperature dependence of resistivity and change in the Fermi surface at the pseudogap critical point of a high- T_c superconductor*, Nat. Phys. 5 (2009), pp. 31–34. (2009).
- ⁷⁰ R. A. Cooper, Y. Wang, B. Vignolle, O. J. Lipscombe, S. M. Hayden, Y. Tanabe, T. Adachi, Y. Koike, M. Nohara, H. Takagi, C. Proust, N. E. Hussey, *Anomalous criticality in the electrical resistivity of $La_{2-x}Sr_xCuO_4$* , Science 323 (2009), pp. 603–607.
- ⁷¹ J. Ayres, M. Berben, M. Čulo, Y.-T. Hsu, E. van Heumen, Y. Huang, J. Zaanen, T. Kondo, T. Takeuchi, J. R. Cooper, C. Putzke, S. Friedemann, A. Carrington, and N. E. Hussey, *Incoherent transport across the strange-metal regime of overdoped cuprates*, Nature 595 (2021), pp. 661–666.
- ⁷² G. Grissonnanche, Y. Fang, A. Legros, S. Verret, F. Laliberté, C. Collignon, J. Zhou, D. Graf, P. A. Goddard, L. Taillefer, and B. J. Ramshaw, *Linear-in temperature resistivity from an isotropic Planckian scattering rate*, Nature 595 (2021), pp. 667–672.
- ⁷³ I. Božović, X. He, J. Wu, and A. T. Bollinger, *Dependence of the critical temperature in overdoped copper oxides on superfluid density*, Nature 546 (2016), 309–311.
- ⁷⁴ N. Doiron-Leyraud, P. Auban-Senzier, S. R. de Cotret, C. Bourbonnais, D. Jérôme, K. Bechgaard, and L. Taillefer, *Correlation between linear resistivity and T_c in the Bechgaard salts and the pnictide superconductor $Ba(Fe_{1-x}Co_x)_2As_2$* , Phys. Rev. B 80 (2009), pp. 214531.
- ⁷⁵ T. M. Rice, *Reviews, prospects and concluding remarks. High- T_c superconductivity-Where next?*, Physica C 282–287 (1997), pp. xix–xxiii.
- ⁷⁶ J. Spalek, M. Fidrysiak, M. Zegrodnik, A. Biborski, *Superconductivity in high- T_c and related strongly correlated systems from variational perspective: Beyond mean field theory*, Phys. Rep. 959 (2022), pp. 1–117.
- ⁷⁷ P. Corboz, T. M. Rice, and M. Troyer, *Competing States in the t - J Model: Uniform d -Wave State versus Stripe State*, Phys. Rev. Lett. 113 (2014), pp. 046402.
- ⁷⁸ L. Spanu, M. Lugas, F. Becca, and S. Sorella, *Magnetism and superconductivity in the t - t' - J model*, Phys. Rev. B 77 (2008), pp. 024510.
- ⁷⁹ See, e.g., the review, B. Edegger, V. N. Muthukumar, and C. Gros, *Gutzwiller-RVB Theory of High Temperature Superconductivity: Results from Renormalised Mean Field Theory and Variational Monte Carlo Calculations*, Adv. Phys. 56 (2007), pp. 927–1033.
- ⁸⁰ B. Edegger, V. N. Muthukumar, C. Gros, and P. W. Anderson, *Electronic Structure of Strongly Correlated d -Wave Superconductors*, Phys. Rev. Lett. 96 (2006), pp. 207002.
- ⁸¹ S. R. White and D. J. Scalapino, *Density Matrix Renormalization Group Study of the Striped Phase in the 2D t - J Model*, Phys. Rev. Lett. 80 (1998), pp. 1272–1275.

- ⁸² N. Nagaosa and P. A. Lee, *Normal-state properties of the uniform resonating-valence-bond state*, Phys. Rev. Lett. **64** (1990), pp. 2450-2453.
- ⁸³ T. K. Lee and S. Feng, *Doping dependence of antiferromagnetism in La_2CuO_4 : A numerical study based on a resonating-valence-bond state*, Phys. Rev. B **38** (1988), pp. 11809-11812.
- ⁸⁴ P. D. Johnson, T. Valla, A. V. Fedorov, Z. Yusof, B. O. Wells, Q. Li, A. R. Moodenbaugh, G. D. Gu, N. Koshizuka, C. Kendziora, Sha Jian, and D. G. Hinks, *Doping and Temperature Dependence of the Mass Enhancement Observed in the Cuprate $Bi_2Sr_2CaCu_2O_{8+\delta}$* , Phys. Rev. Lett. **87** (2001), pp. 177007.
- ⁸⁵ T. Dahm, V. Hinkov, S. V. Borisenko, A. A. Kordyuk, V. B. Zabolotnyy, J. Fink, B. Büchner, D. J. Scalapino, W. Hanke, and B. Keimer, *Strength of the Spin-Fluctuation-Mediated Pairing Interaction in a High-Temperature Superconductor*, Nature Phys. **5** (2009), pp. 217-221.
- ⁸⁶ See, e.g., the review, A. A. Kordyuk, V. B. Zabolotnyy, D. V. Evtushinsky, D. S. Inosov, T. K. Kim, B. Büchner, and S. V. Borisenko, *An ARPES view on the high- T_c problem: phonons vs spin-fluctuations*, Eur. Phys. J. Special Topics **188** (2010), pp. 153-162.
- ⁸⁷ S. D. Wilson, S. Li, H. Woo, P. Dai, H. A. Mook, C. D. Frost, S. Komiya, and Y. Ando, *High-Energy Spin Excitations in the Electron-Doped Superconductor $Pr_{0.88}LaCe_{0.12}CuO_{4-\delta}$ with $T_c=21$ K*, Phys. Rev. Lett. **96** (2006), pp. 157001.
- ⁸⁸ S. D. Wilson, S. Li, P. Dai, W. Bao, J.-H. Chung, H. J. Kang, S.-H. Lee, S. Komiya, Y. Ando, Q. Si, *Evolution of low-energy spin dynamics in the electron-doped high-transition-temperature superconductor $Pr_{0.88}LaCe_{0.12}CuO_{4-\delta}$* , Phys. Rev. B **74** (2006), pp. 144514.
- ⁸⁹ S. D. Wilson, P. Dai, S. Li, S. Chi, H. J. Kang, J. W. Lynn, Nature **442** (2006), pp. 59-62.
- ⁹⁰ K.-J. Xu, J. He, S.-D. Chen, Y. He, S. N. Abadi, C. R. Rotundu, Y. S. Lee, D.-H. Lu, Q. Guo, O. Tjernberg, T. P. Devereaux, D.-H. Lee, M. Hashimoto, Z.-X. Shen, *Anomalous normal state gap in an electron-doped cuprate*, Science **385** (2024), pp. 796-800.
- ⁹¹ X. Ma, M. Zeng, H. Guo, and S. Feng, *Low-temperature T^2 resistivity in the underdoped pseudogap phase versus T -linear resistivity in the overdoped strange-metal phase of cuprate superconductors*, Phys. Rev. B **110**, (2024), pp. 094520.
- ⁹² See, e.g., the review, A. V. Puchkov, D. N. Basov, and T. Timusk, *The pseudogap state in high-superconductors: an infrared study*, J. Phys.: Condens. Matter **8** (1996), pp. 10049-10082.
- ⁹³ B. Bucher, P. Steiner, J. Karpinski, E. Kaldis, and P. Wachter, *Influence of the spin gap on the normal state transport in $YBa_2Cu_4O_8$* , Phys. Rev. Lett. **70** (1993), pp. 2012-2015.
- ⁹⁴ T. Ito, K. Takenaka, and S. Uchida, *Systematic deviation from T -linear behavior in the in-plane resistivity of $YBa_2Cu_3O_{7-y}$: Evidence for dominant spin scattering*, Phys. Rev. Lett. **70** (1993), pp. 3995-3998.
- ⁹⁵ T. Nakano, M. Oda, C. Manabe, N. Momono, Y. Miura, and M. Ido, *Magnetic properties and electronic conduction of superconducting $La_{2-x}Sr_xCuO_4$* , Phys. Rev. B **49** (1994), pp. 16000-16008.
- ⁹⁶ Y. Ando, A. N. Lavrov, S. Komiya, K. Segawa, and X. F. Sun, *Mobility of the doped holes and the antiferromagnetic correlations in underdoped high- T_c cuprates*, Phys. Rev. Lett. **87** (2001), pp. 017001.
- ⁹⁷ J. Kondo and K. Yamaji, *Green's-Function Formalism of the One-Dimensional Reisen berg Spin System*, Prog. Theor. Phys. **47** (1972), pp. 807-818.
- ⁹⁸ See, e.g., S. V. Tyablikov, *Method in the Quantum Theory of Magnetism* (Plenum, New York, 1967).
- ⁹⁹ D. L. Feng, D. H. Lu, K. M. Shen, C. Kim, H. Eisaki, A. Damascelli, R. Yoshizaki, J.-i. Shimoyama, K. Kishio, G. D. Gu, S. Oh, A. Andrus, J. O'Donnell, J. N. Eckstein, and Z.-X. Shen, *Signature of Superfluid Density in the Single-Particle Excitation Spectrum of $Bi_2Sr_2CaCu_2O_{8+\delta}$* , Science **289** (2000), pp. 277-281.
- ¹⁰⁰ H. Ding, J. R. Engelbrecht, Z. Wang, J. C. Campuzano, S.-C. Wang, H.-B. Yang, R. Rogan, T. Takahashi, K. Kadowaki, and D. G. Hinks, *Coherent Quasiparticle Weight and Its Connection to High- T_c Superconductivity from Angle-Resolved Photoemission*, Phys. Rev. Lett. **87** (2001), pp. 227001.